AD_____

Award Number: W81XWH-10-1-0933

TITLE: Ready to Use Tissue Construct for Military Bone & Cartilage Trauma

PRINCIPAL INVESTIGATOR: Francis Y. Lee, MD, PhD

CONTRACTING ORGANIZATION: Columbia University in the City of New York
New York, NY 10032

REPORT DATE: October 2013

TYPE OF REPORT: Annual

PREPARED FOR: U.S. Army Medical Research and Materiel Command
Fort Detrick, Maryland 21702-5012

REPORT DOCUMENTATION PAGE

Form Approved
OMB No. 0704-0188

1. REPORT DATE :	**2. REPORT TYPE:**	**3. DATES COVERED**
October 2013	Annual	30Septmber2012-29September2013

4. TITLE AND SUBTITLE
Ready to Use Tissue Construct for Military Bone & Cartilage Trauma

5a. CONTRACT NUMBER
W81XWH-10-1-0933

5b. GRANT NUMBER
OR090175 - Orthopaedic

5c. PROGRAM ELEMENT NUMBER

6. AUTHOR(S)
Francis Y. Lee, MD, PhD

E-Mail: fl127@columbia.edu

5d. PROJECT NUMBER

5e. TASK NUMBER

5f. WORK UNIT NUMBER

7. PERFORMING ORGANIZATION NAME(S) AND ADDRESS(ES)
Trustees of Columbia University in the City of New York
Columbia University Medical Center
650 West 168th Street, New York, NY 10032

8. PERFORMING ORGANIZATION REPORT NUMBER

9. SPONSORING / MONITORING AGENCY NAME(S) AND ADDRESS(ES)
U.S. Army Medical Research and Materiel Command
Fort Detrick, Maryland 21702-5012
JENNIFER.SHANKLE@US.Army.Mil
301-619-2193

10. SPONSOR/MONITOR'S ACRONYM(S)

11. SPONSOR/MONITOR'S REPORT NUMBER(S)

12. DISTRIBUTION / AVAILABILITY STATEMENT
Approved for Public Release; Distribution Unlimited

13. SUPPLEMENTARY NOTES

14. ABSTRACT

Our proposal "Ready-to-Use Tissue Construct for Military Bone and Cartilage Trauma" addresses the current limitations in treating complex, high-energy musculoskeletal wounds incurred in active combat. High-energy blast-injuries produce immediate, short-term and long-term consequences such as acute limb loss, bone loss, cartilage loss, stiffness, limping, pain, arthritis, and permanent disability, often requiring multiple reconstructive surgeries and prolonged rehabilitation. These 'osteochondral health' issues ultimately affect a soldier's quality of life both during active service and after retirement. Tissue engineering technology is a rapidly evolving field and utilizes mesenchymal cells, tissue scaffolds and growth factors. However, there are no currently available tissue-engineering constructs exhibiting 'Ready-to-Use' functionality. The most significant barrier to the practical application of tissue engineering for combat-related bone and cartilage defects is the *time- and labor-intensive process of mesenchymal stem cell expansion*. The **goal** of this proposal is to introduce a new tissue engineering paradigm to the Defense Health Program (**DHP**) by utilizing a biomechanically competent and anatomically matched tissue construct without resorting to the cumbersome process of mesenchymal stem cell expansion.

15. SUBJECT TERMS
Ready to use tissue construct, biomechanically competent anatomically matched tissue construct

16. SECURITY CLASSIFICATION OF:			**17. LIMITATION OF ABSTRACT**	**18. NUMBER OF PAGES**	**19a. NAME OF RESPONSIBLE PERSON**
					USAMRMC
a. REPORT	**b. ABSTRACT**	**c. THIS PAGE**			**19b. TELEPHONE NUMBER** *(include area code)*
U	U	U	UU		

Table of Contents

1. INTRODUCTION (excerpted from grant)

Our study "Ready-to-Use Tissue Construct for Military Bone and Cartilage Trauma" addresses current limitations in treating complex, high-energy musculoskeletal wounds incurred in active combat. High-energy blast-injuries produce immediate, short-term and long-term consequences such as acute limb loss, bone loss, cartilage loss, stiffness, limping, pain, arthritis, and permanent disability, often requiring multiple reconstructive surgeries and prolonged rehabilitation. These 'osteochondral health' issues ultimately affect a soldier's quality of life both during active service and after retirement. Tissue engineering technology is a rapidly evolving field and utilizes mesenchymal cells, tissue scaffolds and growth factors. However, there are no currently available tissue-engineering constructs exhibiting 'Ready-to-Use' functionality. The most significant barrier to the practical application of tissue engineering for combat-related bone and cartilage defects is the *time- and labor-intensive process of mesenchymal stem cell expansion*. The goal of the current study is to introduce a new tissue engineering paradigm to the Defense Health Program (DHP) by utilizing a biomechanically competent and anatomically matched tissue construct without resorting to the cumbersome process of mesenchymal stem cell expansion. Our project utilizes a series of *in vivo* large animal translational experiments that will hopefully lead to the development of new military technology products and utilities for the definitive and preventive orthopaedic care of military personnel and retirees. The project has 3 major aims, excerpted from the revised Statement of Work and listed below:

Aim 1. To examine whether our prefabricated constructs can reconstitute osteochondral defects of critical-size in a canine distal femoral condyle defect model simulating high-energy blast-injury. Osteochondral injuries of any size require anatomically perfect reconstruction to prevent pain and post-traumatic arthritis. We hypothesize that anatomically-conforming osteochondral constructs with controlled release of TGF-β3 can reconstitute physiologic *hyaline cartilage*-osseous transition in massive osteochondral defects in large animals. We will conduct functional outcome analysis, X-ray/MRI examination and histologic analysis.

Aim 2. To examine whether our prefabricated construct can reconstitute critical size segmental defects in canine tibiae. Critical-size segmental defects in long bone diaphyses require extensive reconstructive procedures and prolonged rehabilitation times. We hypothesize that our *Ready-to-Use* constructs can successfully restore 3 cm critical size segmental defects in dog tibiae. We will examine the incorporation and regeneration of the biogenic implant with host bone by conducting functional outcome assessments, radiography, biomechanical torsional testing and histologic examination.

Aim 3. To examine biomechanical suitability of ready-to-use constructs in massive osteochondral defects and segmental bone defects in human cadaveric femora. We have successfully developed anatomically conforming bone and cartilage constructs for rats and rabbits. Early joint motion and ambulation are important in human patients. We hypothesize that our *ready-to-use* construct can maintain the biomechanical and functional properties in human cadaveric bones under simulated physiologic load. We intend to optimize and adapt our "ready-to-use" scaffold construct for humans. We will verify the biomechanical competence in a critical size defect in human femora and knee joints by simulating loads seen during ambulation and knee range of motion.

Our central hypothesis is that an anatomically and biomechanically compatible scaffold with TGF-β3 and BMP-2 can reconstitute massive cartilage/bone defects without exogenous MSCs. The goal of this Technology Development Project is to simplify the current paradigm of tissue engineering by 1) eliminating the need for time- and labor-intensive stem cell harvesting and expansion and 2) adopting anatomically conforming constructs which promote incorporation, remodeling, early joint motion, partial weight bearing, and ambulation. Our hypothesis is based on compelling preliminary data in small animal models, such as mice, rats and rabbits. The current protocol will take another step towards military application by verifying successful regeneration of cartilage (**Aim 1)** and bone (**Aim 2**) in massive canine bone defects and by confirming biomechanical and functional suitability in human cadaveric knee and tibia defect models (**Aim 3**). **Aim 1** and **Aim 2** are significant in that they will introduce a simpler, more cost-effective approach to tissue engineering that obviates the need for extensive cell culturing and laboratory support. **Aim 3** is significant in that the injured soldiers can start early rehabilitation and ambulation following reconstructive surgeries using Ready-to-Use anatomically and biomechanically conforming biogenic scaffolds.

2. BODY

2.0 Overview

Our current Columbia and USAMRMC Animal Care and Use Review Office (ACURO) approved IACUC protocol has two components, reflecting Aim 1 (osteochondral defects) and Aim 2 (segmental defects) of the grant. The approved IACUC protocol permits 3 pilot dogs for Aim 1 and 3 pilot dogs for Aim 2. Several minor modifications to the original IACUC protocol were required which are provided in the Appendix. All the pilot dogs were to receive scaffolds composed of 90% poly-caprolactone (PCL) and 10% hydroxyapatite (HA) by weight (PCL+HA) without any seeding with either canine MSC or biologic agents (TGF-β3 for Aim 1 or BMP for Aim 2). The purpose of the pilot surgeries was twofold, a) to demonstrate the ability of the surgical team to perform the surgery and that the surgery did not result in excessive pain and discomfort to the animal and b) to demonstrate that there was no immune response to the implanted scaffolds. All three surgeries were performed for Aim 2 in May and June of 2012. Two of the three animals were taken to the full 16 week duration of the experiment and then were humanely sacrificed. Biomechanical testing was performed on their 4 hind limbs. The third Aim 2 dog had an untoward event that required it to be humanely sacrificed approximately 1 week post-surgery.

The three Aim 1 pilot dogs operated in September and October of 2012 successfully completed their 16 weeks of post-surgery recovery period and were sacrificed. Monthly post-op MRI images were obtained for the three osteochondral defect dogs and three-dimensional models were created to establish a chronologic history of bony ingrowth/articular cartilage growth in the osteochondral dogs. No biomechanical testing was performed because there was no tissue growth on the articular surfaces of the osteochondral scaffolds in all three dogs. In lieu of biomechanical testing, hard tissue histology was performed for the left (experimental) distal femora of the three dogs.

Surgeries were performed on six additional segmental defect dogs. Two dogs received canine allografts, one received a plain scaffold and three received scaffolds attached with microspheres containing BMP-2. The scaffold dog experienced premature plate bending and needed to be sacrificed early. Both allograft dogs successfully completed their 16 post-op healing periods and were sacrificed and mechanically tested. Following evaluation of the segmental dog with the bent plate, a slightly broader plate was selected and used in three additional dogs that received the microspheres with BMP-2. The BMP segmental defect dogs are partially through their 16 week recovery period at the writing of this report and are doing well. Radiographs were taken on a bi-weekly basis for all segmental defect dogs to document the progression of bony healing. Outcome measures were recorded throughout the 16 week experimental period for all dogs. CT images were obtained of the hind limbs of the postmortem segmental defect dogs and three-dimensional models were created to assess bony ingrowth. Histology was performed for the osteochondral dogs and for the tested segmental dogs following mechanical testing.

Mechanical testing for the segmental component of Aim 3, testing of the scaffold in human cadaveric specimens to determine the strength of the bone-scaffold-plate construct immediately post-op, was completed. An additional study arm that compared the effect of locking versus non-locking fixation for the bone-scaffold-plate construct was also completed using 6 matched pairs of human fresh-frozen tibiae.

The subsections to follow will elaborate on the above accomplishments and experimental results.

2.1 Aim 1 - Osteochondral Defects

Surgeries were performed on the first three osteochondral defect dogs in September and October of 2012, as detailed in the progress report for last year. As per the protocol, radiographs were taken immediately post-op, and at post-op weeks 2, 4, 8, 12, 16. MR imaging was also performed monthly. The dogs were sacrificed after week 16 post-op and histology was performed.

2.1.1 Osteochondral Defect Scaffold

The implant design used was detailed in the previous progress report, with a "hat" whose curvature approximately matched that of the canine medial condyle from the region shown in Figure 1, with a size of approximately 13 x 6 x 9 mm^3 and a tapered keel (9 mm by 4 mm by 4 mm) to provide stability to the implant and prevent any rotation of the implant. The location, and hence curvature of the implant surface, was selected to place the implant in the load bearing region of the canine knee joint (2) while still allowing access to the joint without disrupting the main ligaments of the

knee. The implant consisted of a two layer Polycarprolacton (PCL) mixed with 10% hydroxyapatite (HA) scaffold with a 500 μm top layer with a pore size of 400 μm to promote articular cartilage growth. It was not seeded with any material or cells for the first three osteochondral dogs. A second layer with a pore size of 200 μm, as shown in Figure 2, was provided to support bony ingrowth from the surrounding subcondral bone.

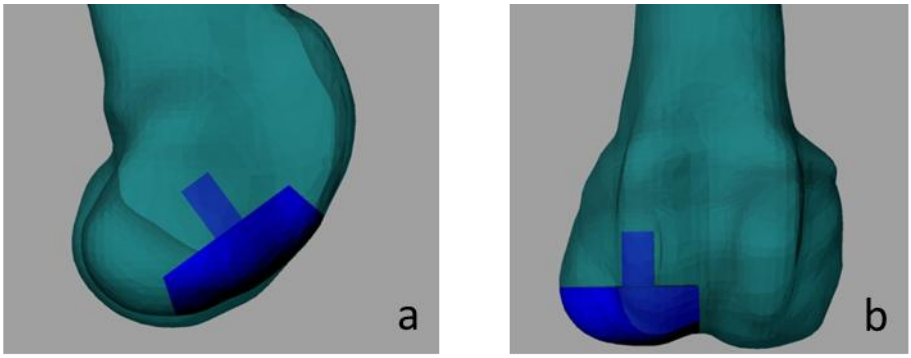

Figure 1: computer model of osteochondral scaffold virtually implanted in a 3-D computer model of the medial condyle of left canine knee, a) medial to lateral direction, b) anterior to posterior direction

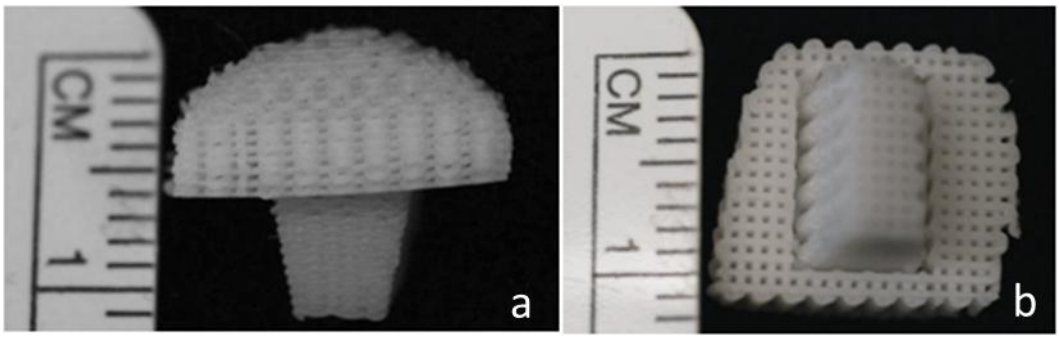

Figure 2: Osteochondral scaffold showing a) side view in superior-inferior direction, b) keel of scaffold

2.1.2 Outcome Measures for Osteochondral Defect Dogs

Outcome measures of gait, lameness, pain, knee motion and an aggregate of these measures were recorded for Osteochondral Defect Dogs 1, 2 and 3 every weekday, excluding Saturdays and Sundays and reported below in Figures 3, 4, and 5, respectively. The criteria used to determine the outcome measures are provided in Table 1. However, because sling walking was prescribed immediately following surgery, no outcome measures were obtained until Day 10 for all three dogs. Figure 3 shows that Dog 1 had a steady improvement in its aggregate outcome score until approximately 40 days post-surgery. After that point, the aggregate outcome score leveled off and remained somewhat constant until sacrifice. Figure 4 shows that Dog 2 started out with a relatively high total outcome score, but then the score degraded at about day 30 post-op and remained low until sacrifice. Figure 5 shows that Dog 3 had a steady improvement in its total outcome score until approximately day 30 post-op, after which the score plateaued and remained relatively high until sacrifice.

Clinical observation of the dogs was consistent with the outcome measures. Dogs 1 and 2 were observed to have lateral patella subluxation, with Dog 2 consistently dislocating its patella. Dog 3 exhibited no obvious patella subluxation. Post-mortem observations, reported in Section 2.1.6 below further support these findings. The surgeries for Dogs 1 and 2 were performed by one surgeon whereas the surgery for Dog 3 was performed by a different surgeon. The first surgeon performed a wide incision and exposure to place the scaffold for Dogs 1 and 2 whereas the second surgeon used a minimally invasive surgical approach with a much smaller incision and far less disruption to the patella ligaments and surrounding soft tissues. It is speculated that the reattachment of the medial patella femoral ligaments for Dogs 1 and 2 was inadequate, resulting in the lateral subluxation of their patellae. With much less soft tissue disruption, Dog 3 appeared not to experience any patella subluxation.

Outcome	Criteria	Range
Gait	Non weight-bearing	0
	Partial weight-bearing	1
	Full weight-bearing	2
Lameness	Does not use limb during walking	0
	Partial use of affected limb, walks with noticeable limb	1
	No lameness when walking	2
Pain	Severe reaction to touch, withdraws upon the slightest touch with guarding behavior and/or vocalization	0
	Mild reaction to touch, withdraws limb upon touch	1
	No reaction to touch of affected limb	2
Knee Motion	Significant reduction in range of motion (0-30%)	0
	Moderate reduction in range of motion (30-60%)	1
	Slightly reduced range of motion (60-80 %)	2
	Normal range of motion (90-100%, preoperative range)	3
Total		0-9

Table 1: Criteria used to grade Outcome Measures for both Osteochondral Defect and Segmental Defect Dogs.

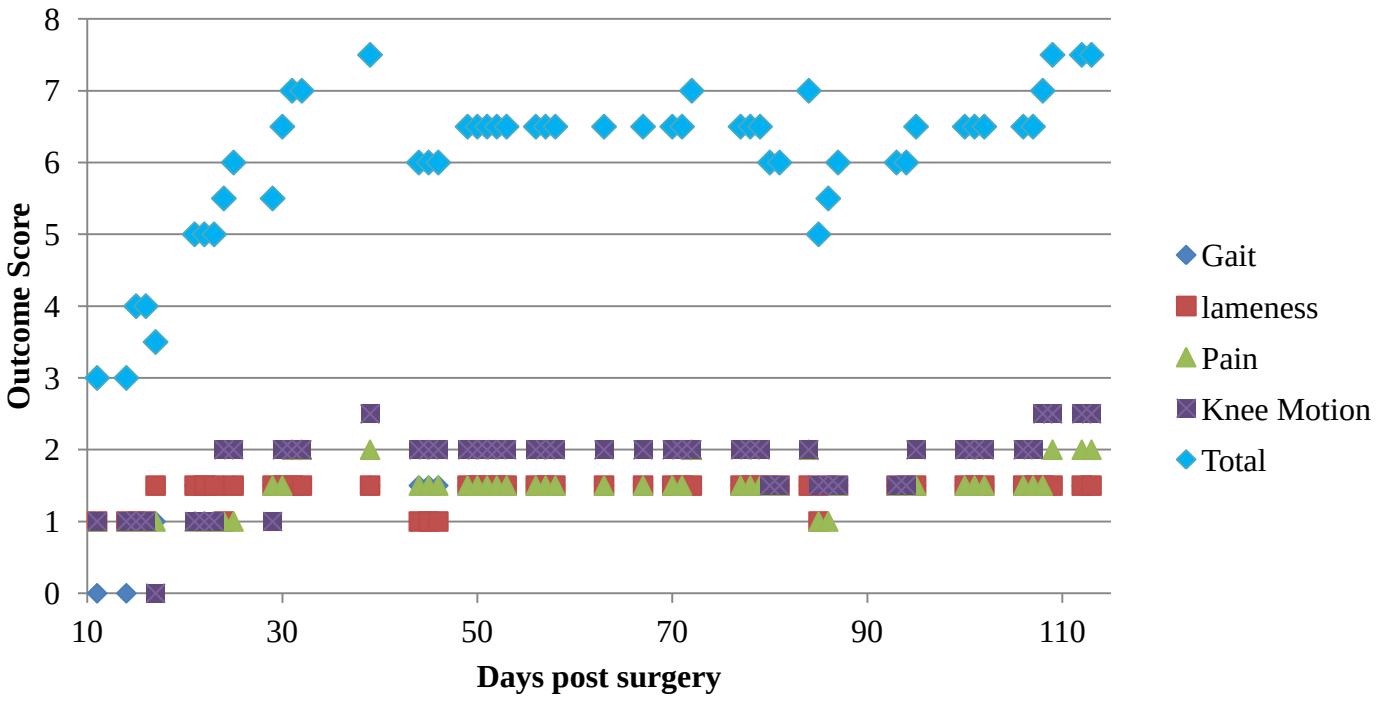

Figure 3: Outcome measurement for Osteochondral Defect Dog 1.

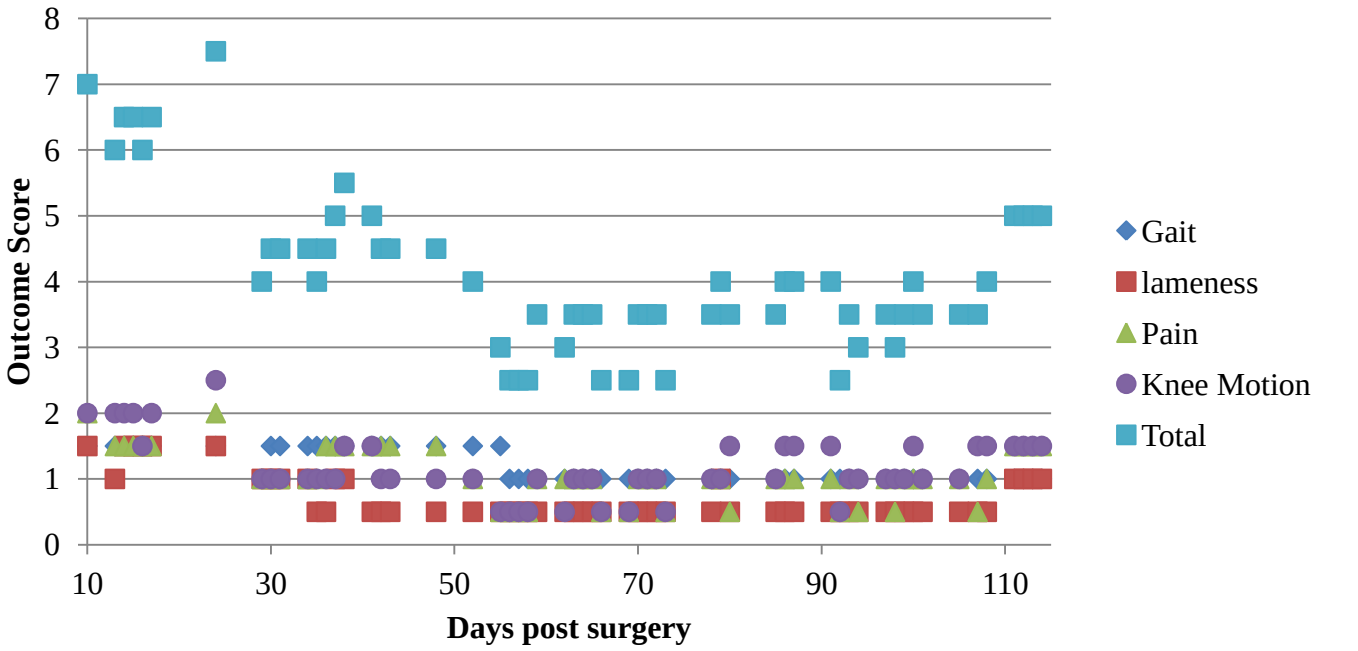

Figure 4: Outcome measurement for Osteochondral Defect Dog 2.

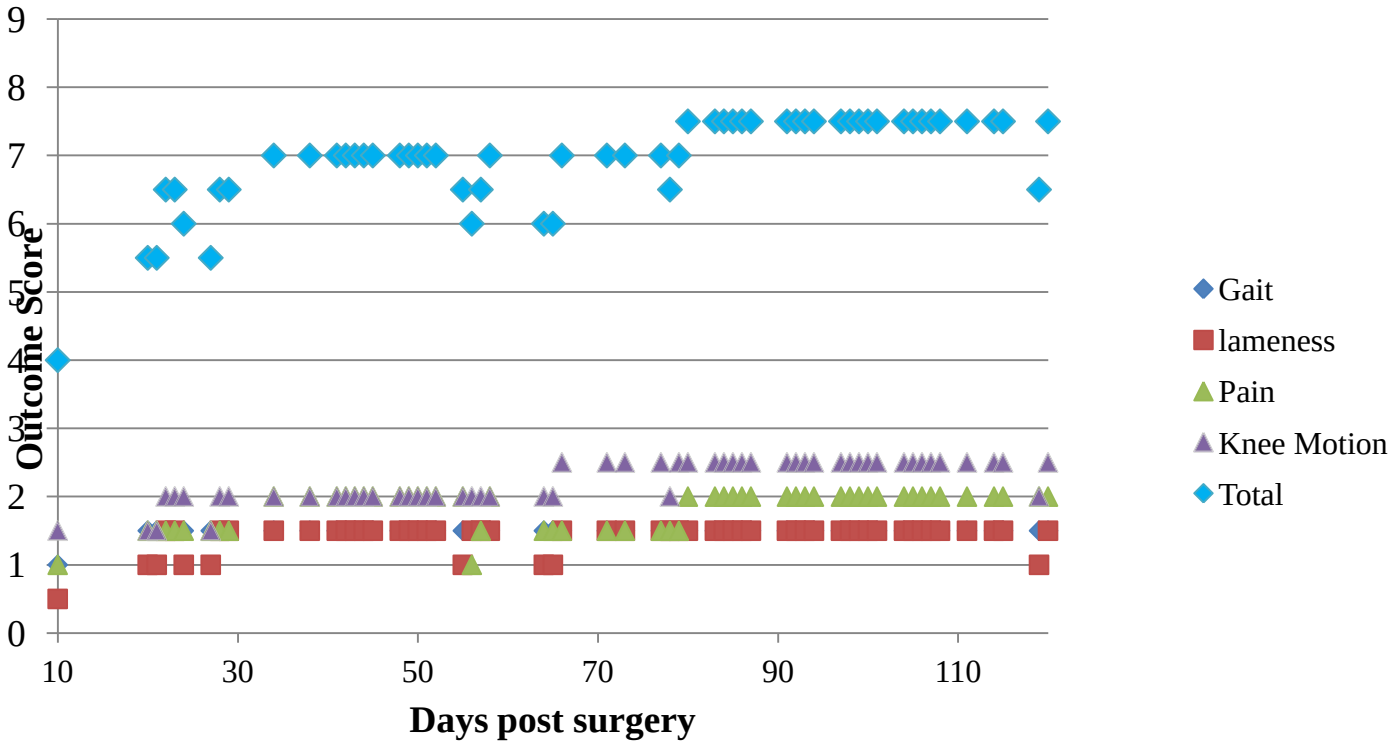

Figure 5: Outcome measurement for Osteochondral Defect Dog 3.

2.1.3 Osteochondral Defect Radiographs

Radiographs of Osteochondral Defect Dogs 1, 2 and 3 as a function of time are provided in Figures 6, 7 and 8, respectively. The outline of the scaffold trough can be seen in the radiographs and is highlighted by red circles in the posterior-anterior views. For all three dogs, the radiographs demonstrate the large surgically created bony defect at time 0 in the area of the scaffold. By week 4 there is some blunting at the scaffold-bone interface indicative of bony ingrowth. This progresses through week 16 indicating continued osseous integration. In these unloaded scaffolds the articular surface remains radiolucent indicating little tissue formation.

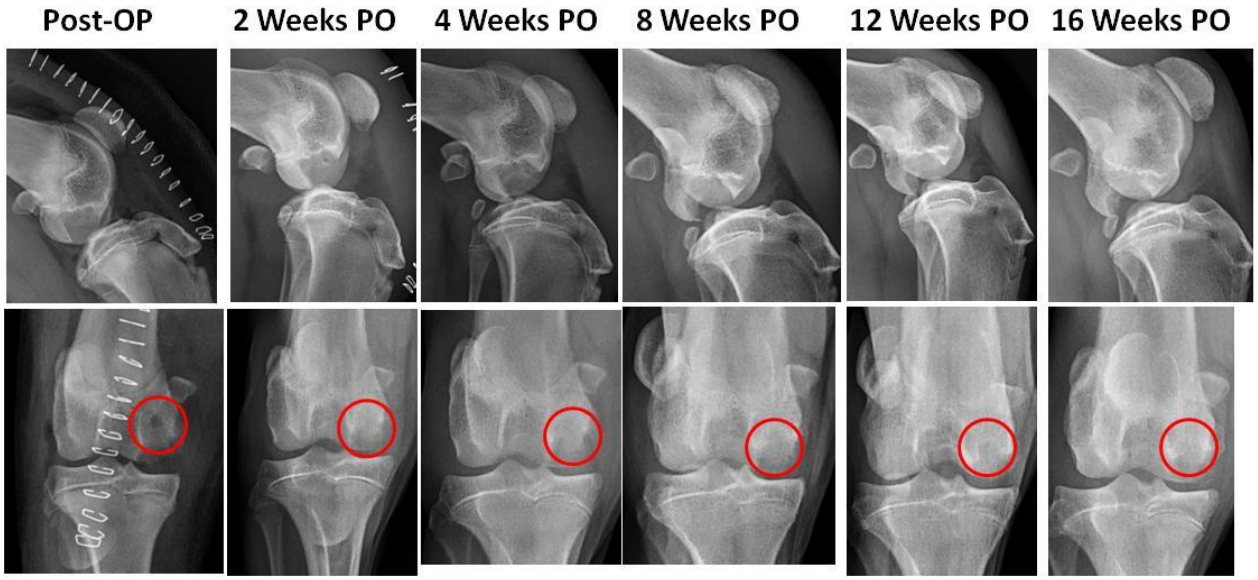

Figure 6: Radiographs for Osteochondral Dog 1 as a function of time; top row: medial-lateral view; bottom row: posterior-anterior view.

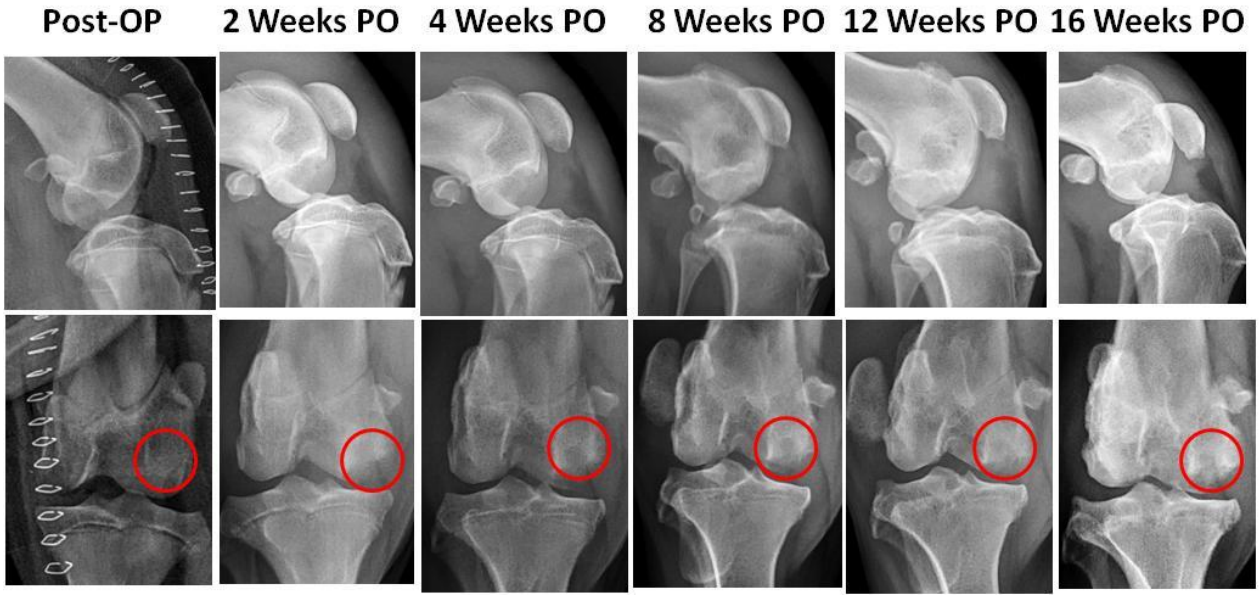

Figure 7: Radiographs for Osteochondral Dog 2 as a function of time; top row: medial-lateral view, bottom row: posterior-anterior view.

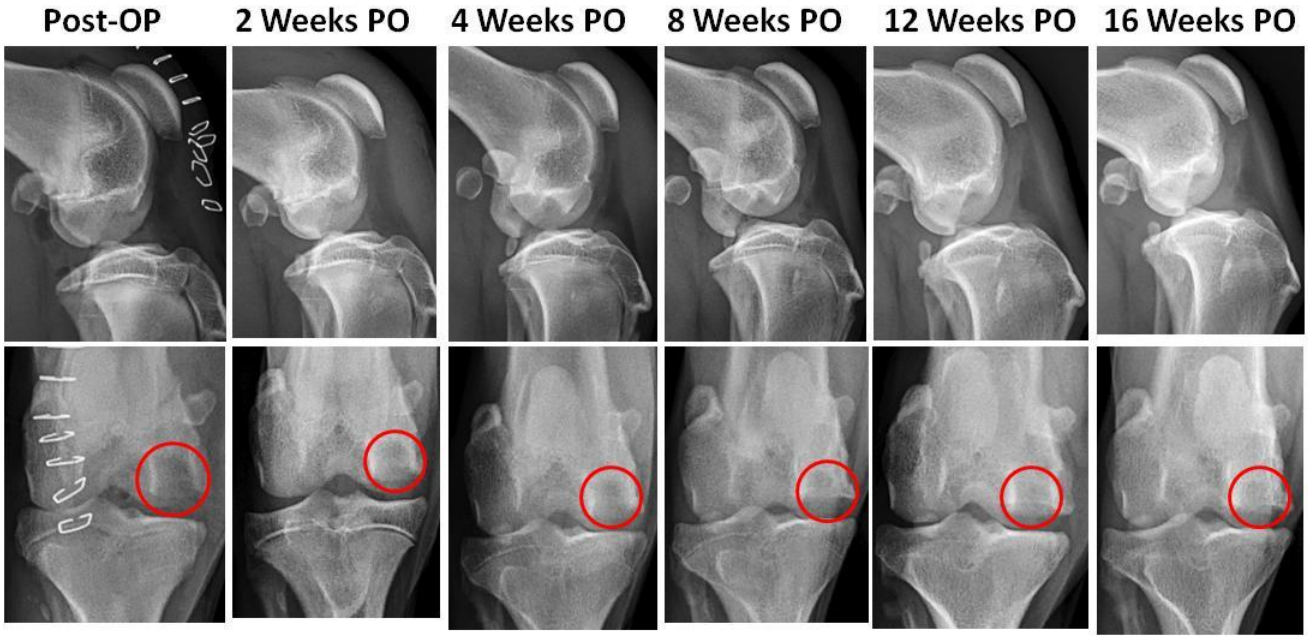

Figure 8: Radiographs for Osteochondral Dog 3 as a function of time: top row: medial-lateral view, bottom row: posterior-anterior view.

2.1.4 Osteochondral Defect MR Imaging

T1 and T2 MR images of Osteochondral Defect Dogs 1, 2 and 3 as a function of time are provided in Figures 9, 10 and 11, respectively. There was no apparent cartilage growth on the surface of scaffolds even at week 16. There were no apparent changes in the MR images as post-op time progressed. The red circles clearly outline the trough created in the condyle to receive the scaffold keel, which appear black in the MR image. A three-dimensional model of the distal femur of Osteochondral Dog 1 at post-op week 4 is shown in Figure 12. The sectioned condyle and trough created in the bone is apparent. The PCL-HA scaffold does not appear in the MR images and hence a model of it cannot be created from the MR images. The T1 MR images demonstrates low signal of the scaffold and sharp edges at the initial post-op 4 week. In agreement with the radiographic findings there is progressive blunting of the implant bone interface indicating some bony ingrowth.

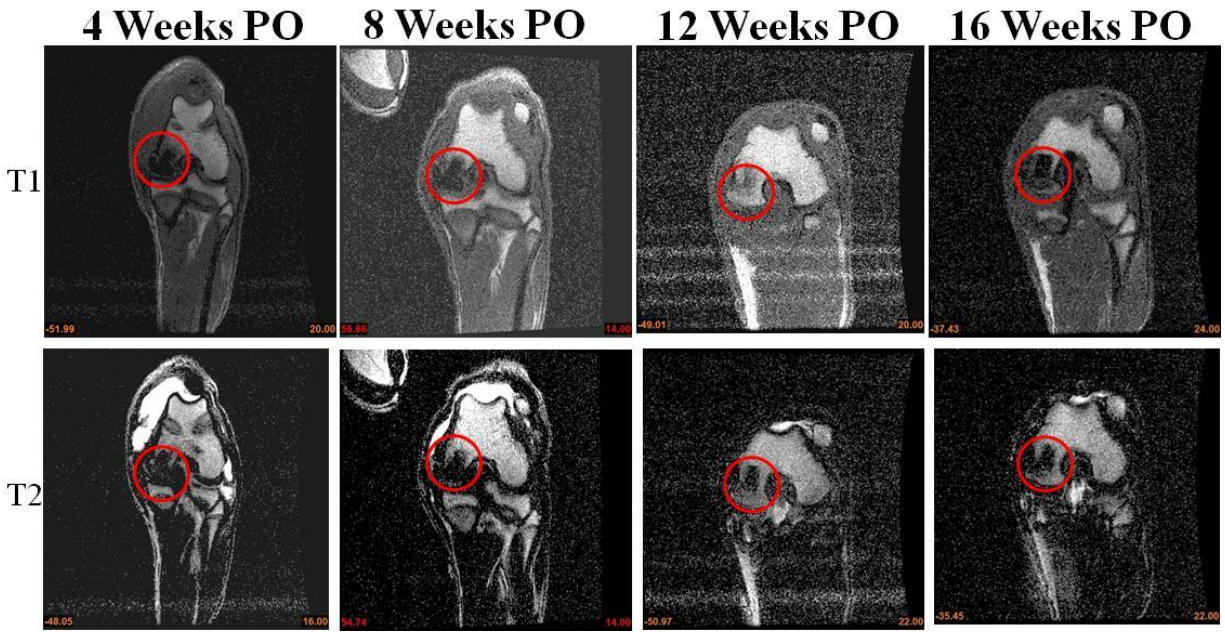

Figure 9: MR images of Osteochondral Dog 1 as a function of time: top row: T1 signal, bottom: T2 signal

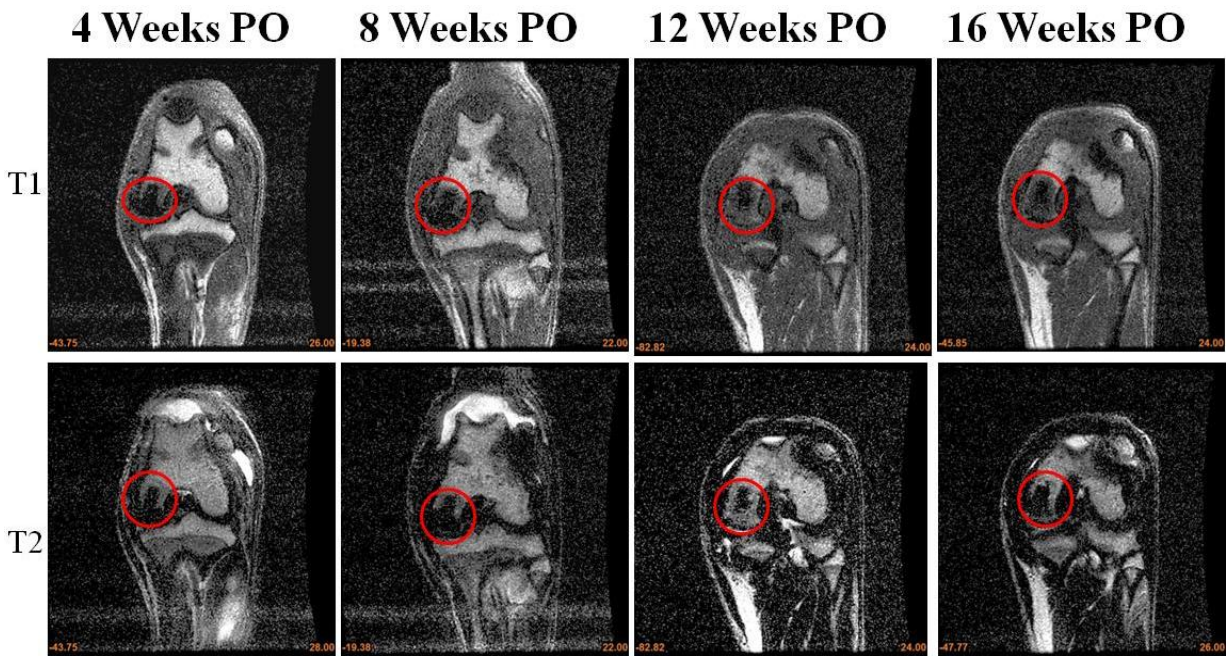

Figure 10: MR images of Osteochondral Dog 2 as a function of time: top row: T1 signal, bottom: T2 signal

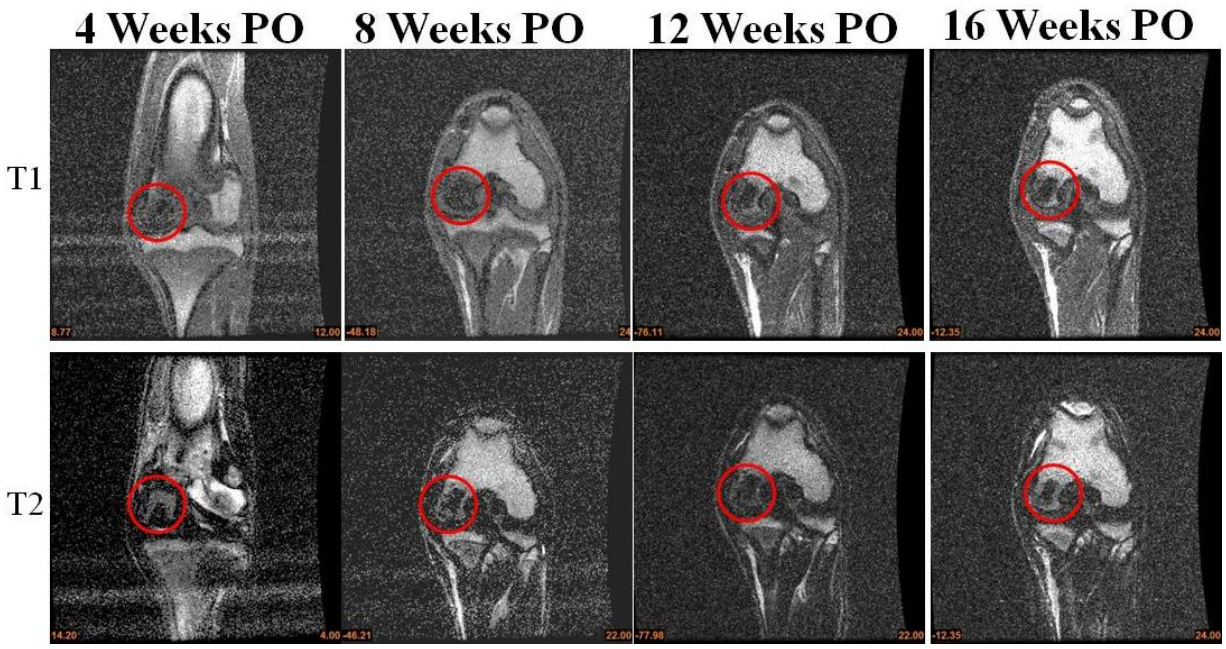

Figure 11: MR images of Osteochondral Dog 3 as a function of time: top row: T1 signal, bottom: T2 signal

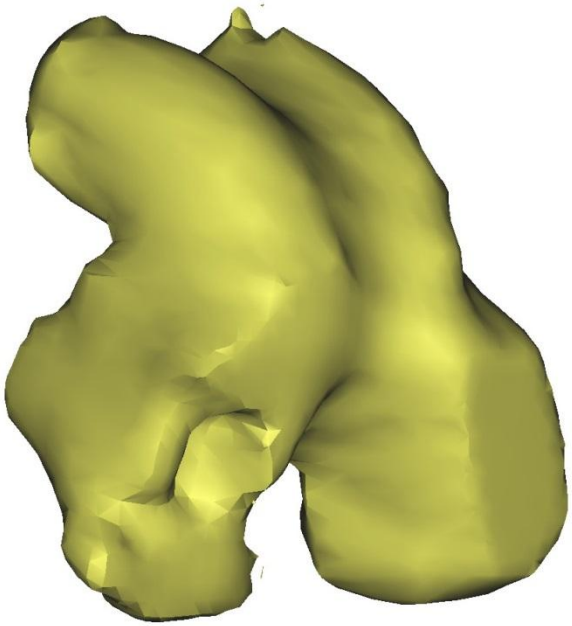

Figure 12: 3-D computer model of experimental left knee of Osteochondral Defect Dog 1 on Post-op week 4.

2.1.5 Post-mortem Observations for Osteochondral Defect Dogs

Following the prescribed 16 week post-op recovery period, all three osteochondral defect dogs were sacrificed and the intact joint capsules of both the experimental and contralateral control legs were carefully dissected out. The maximum flexion angle of each dog was measured. All three dogs had a maximum flexion angle of approximately 120˚ for the contralateral (control limb). The maximum flexion angle of the experimental limb for all three dogs was slightly less than that of their control limb, as shown in Figure 13.

Following the flexion angle measurement, the joints were disarticulated. The intra-operative photographs of the medial condyles with the scaffold implants are repeated from last year's report in Figure 14 (top row). The bottom row of Figure 14 shows the post dissection images. As mentioned above, Osteochondral Dogs 1 and 2 experience significant patella subluxation and frequent patella dislocation for Dog 2. The repeated trauma caused by the patella dislocations resulted in the generation of a synovial pannus on the surfaces of the lateral condyles of the knees shown in dissection Figure 14 (a) and (b), bottom row, as well as malformations of the patella grooves and assorted osteophytes. The apparent damage to these knees is consistent with the lower outcome scores for these dogs and the clinically observed limp that these dogs occasionally exhibited. However, the articular surfaces of Osteochondral Dog 3, which was not observed to have any noticeable patella subluxation, appear relatively normal. Osteochondral Dog 2 was also somewhat heavier (>55 lbs) than that of Dogs 1 and 3 which may have exacerbated this effect, leading to the very poor condition of this knee. As mentioned above, it is suspected that the much larger surgical exposures for Dogs 1 and 2 than for Dog 3 is the main cause for the patella subluxations/dislocations and the resulting damage to the knees.

The prominence of the osteochondral scaffold above the native articular surface can be seen in Figure 14, top row for all three dogs. It is suspected that this prominence led to the breakdown of some of the top regions of the scaffold, as can be seen from the fine strands of PCL+HA extending from the scaffolds. This is most obvious for Dog 1, but was present for all three dogs. Scratches to the opposing medial tibial plateau were observed that further supports the potential abrasive effect of having the scaffolds seated proud. It is thought that this surface shearing effect may have prevented any soft tissue from forming on the articular surface of the scaffold. However, it is also possible that the plain scaffold may not lend itself to soft tissue formation on the articular surface. Care will be taken in the subsequent osteochondral defect surgeries to ensure that the articular surface of the implant is at least 1-2 mm below that of the native articular cartilage to avoid any surface shear and to allow us to better answer the question of whether or not soft tissue can form on the articular surface of the plain scaffold.

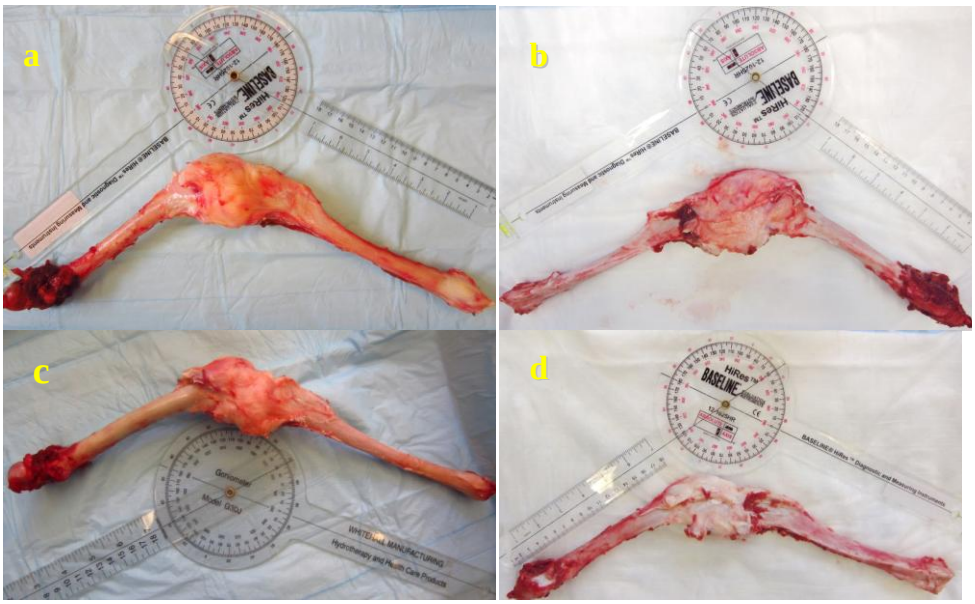

Figure 13: Maximum knee flexion angle of Osteochondral Defect dogs with capsule, tendon and patella, (a) Dog 1: 113°, (b) Dog 2: 114°, (c) Dog 3: 132°, (d) Dog 2 contralateral control: 120°.

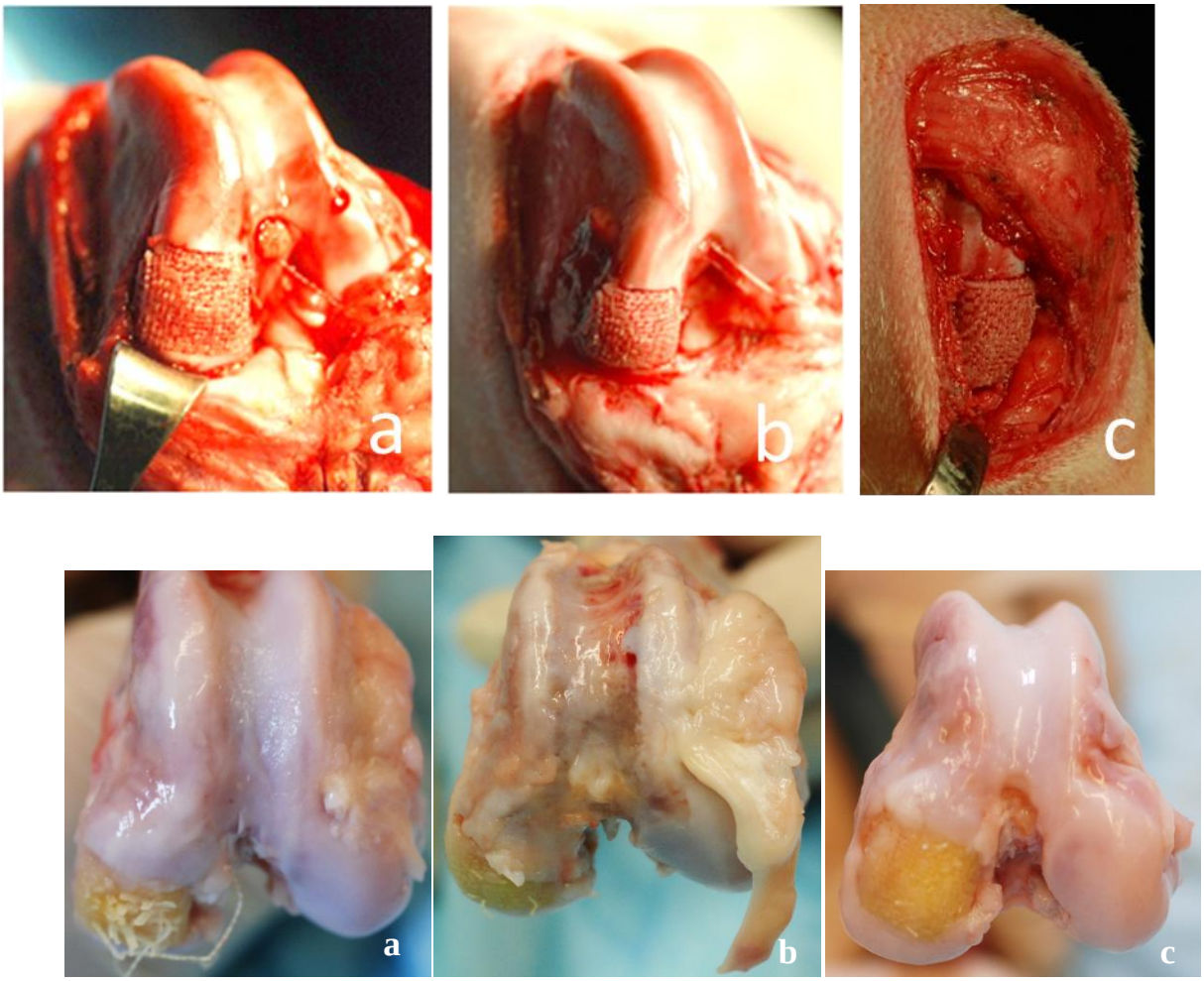

Figure 14: Inferior view of Osteochondral Defect dogs: (a) Dog 1, (b) Dog 2, (c) Dog 3. Top row: intraoperative view. Bottom row – view following dissection.

2.1.6 Osteochondral Defect Hard Sectioning Histology Study

Preparation

After dissection and photographing, the entire knee condyles of the three osteochondral dogs were sectioned and immediately immersed in 10% formalin solution for two months for fixation. Following fixation, the condyles underwent automatic dehydration and plastic infiltration (Leika TP 1020, Germany). The samples were put in a mold and covered with Technovit 7200 media (EXAKT, Germany). The submersed samples were than exposed to yellow and blue light Light Polymerization Utility (EXAKT, Germany) for a period of two days to create a hard specimen block. The specimen block was then trimmed with a band saw (EXAKT, Germany), and the cut surface was ground smooth with 800 or 1000 grit sandpaper. The smoothed side was then glued to a 4"× 2" plastic template slide by Technovit 7210 and the glue was hardened on a Light-Polymerization-Block-Sandwich machine (EXAKT, Germany) with blue light for 5 min. The process was repeated for the other side to create a specimen block sandwich. The block was then cut on a band saw with a 1 cm-wide diamond blade (EXAKT, Germany). The cut direction was parallel to the surface to be stained resulting in a 800~1000 μm thick slide specimen. To prepare the specimen for staining, the surface underwent a series of progressively finer polishings using 800 grit paper, 1000 grit paper and 1200 grit paper until only a 50~80 μm specimen layer was left. To eliminate scratches from cutting and grinding and to improve transparency of the slide surface, the specimen surface was polished with 4000 polish paper for more than one hour on the same grinding machine. The entire protocol followed the method provided by the EXAKT company (1).

The slides were then stained with the standard Haematoxylin & Eosin (H&E) Stain or Masson's Trichrome Stain to distinguish connective tissues.

Microscopic Imaging

The hard tissue histology images were viewed with a Leica Microscope under 2X magnification. A montage was created from a number of 2X images using the Leica software and is shown in Figure 15a. Figure 15b shows a zoom-in view of the scaffold and the surrounding native bone chopped from the original large montage image generated by Leica software. Figure 16 shows the same region stained with Masson's Trichrome. From Figures 15 there appears to be tissue ingrown (darker pink) at the scaffold / native bone interface, with very light pink being the PCL+HA scaffold material. From Figure 16, there also appears to be some tissue ingrowth. However, there is no cartilage formation on the articular surface of the unseeded scaffold. This may be due to either an inability of the plain scaffold to incorporate chondrocytes, or it may be because, as is apparent in Figure 15(a), the scaffold was placed proud, and therefore there was a continuous shear of the scaffold surface against the tibia, possibly preventing any soft tissue from forming on this surface. Similar histological results were obtained for Osteochondral Dogs 2 and 3.

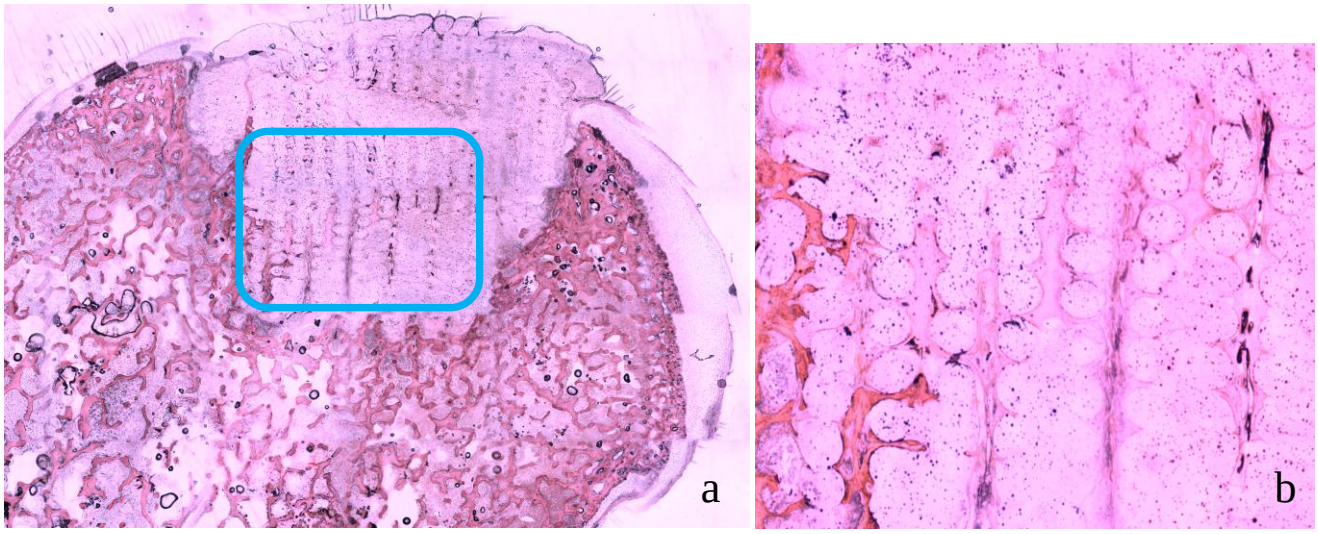

Figure 15: Hard sectioning histology image of Osteochondral Dog 1, stained by H&E method. (a) Montage of entire knee condyle. (b) Close-up of enclosed area showing the scaffold and adjacent native bone.

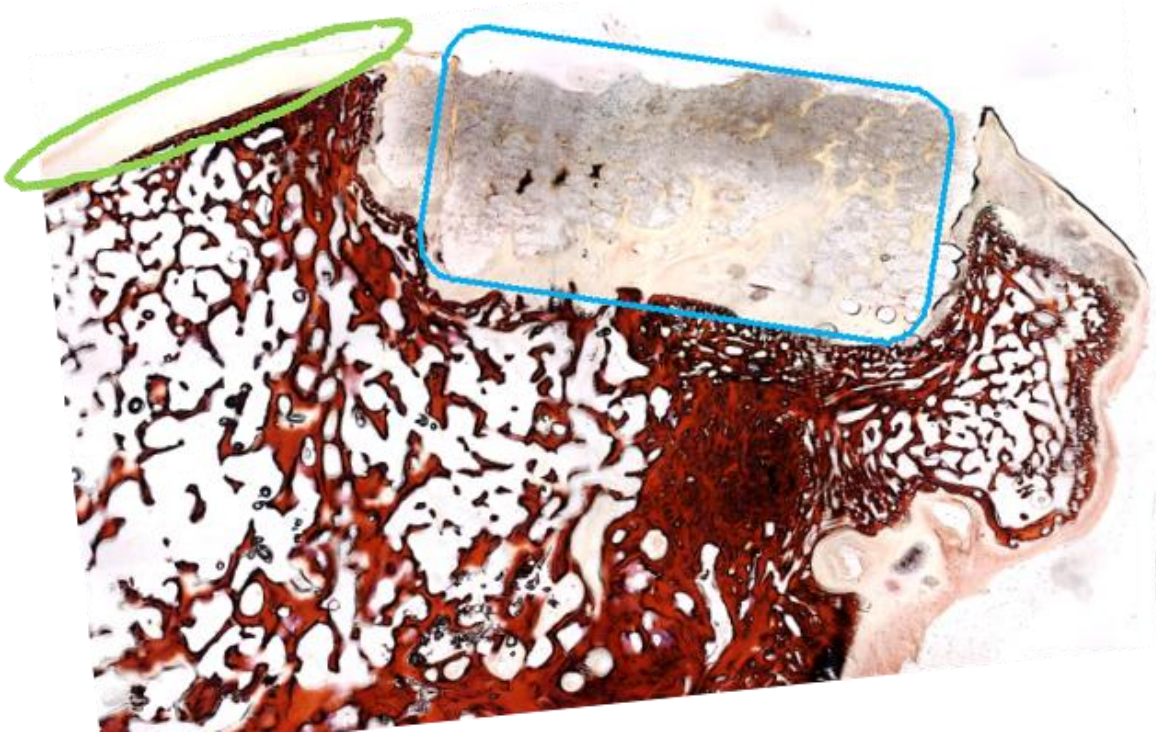

Figure 16: Hard sectioning histology image of Osteochondral Dog 2, stained with Masson's Trichrome. The region enclosed by the green oval is native articular cartilage, the region enclosed by blue represents the PCL+HA scaffold.

2.2 Aim 2 - Segmental Defects

The results for Segmental Defect Dogs 1 and 2 were reported in the 2012 annual report. Segmental Defect Dog 3 experienced plate bending and was sacrificed early as reported in the 2012 annual report. A slightly different type of LCP plate was recommended and compared to the originally used plated via mechanical testing. Results of study are reported in Section 2.2.3. Modifications of the Columbia IACUC were approved that increased the allowable segmental dog number to the full experimental number in the grant (40) less one dog, apparently due to a numerical mistake by the IACUC. A modification will be submitted to correct this minor mistake. Accordingly, surgeries were performed on Segmental Defect Dogs 4, 5, 6, 7, 8, 9 and 10 during this reporting period. Dogs 4 and 7 received unseeded scaffolds, Dogs 5 and 6 received canine allografts and Dogs 8, 9 and 10 received scaffolds seeded with microspheres containing BMP-2. Details are provided below. Radiologic and CT images of the hind limbs following surgery were obtained for all dogs. Outcome measures were recorded daily for both dogs throughout the 16 week recovery period.

2.2.1 Segmental Defect Scaffold Design

The objective of the segmental defect scaffold is to promote bony ingrowth into the subchondral bone. The segmental defect scaffold architecture is based on the work of Lee et al, (Lancet 2010) (2) researchers on this grant. In contrast to the osteochondral defect design reported above, the segmental defect scaffold has the same pore size throughout. The scaffold has no outer cortex layer and an 8 mm lumen to permit the infusion of bone marrow material through the lumen and into the scaffold through the surface pores, Figure 17. The scaffolds were made 20 mm long to represent a critical size defect in the dog (2).

Surgeries were performed on Segmental Dog 4 in November 2012 and Dog 7 in May 2013 with two unseeded scaffolds. Those two scaffolds were made with the 3-D printer (Bioplotter, EnvisionTec, Germany) using a 25G needle. The molecular weight (MW) of the PCL used in the previous scaffolds was 60,000 (SigmaAldrich Co. USA), however, this product was discontinued in 2013. To produce scaffolds with similar strength as the 60,000 MW based scaffolds, a mixture of PCL materials with MW 45,000 and MW 90,000 in a1:2 ratio was decided upon after numerous attempts with a variety of different mixtures of the two molecular weight PCL products. In addition, the size of the dispensing needle in the 3-D printer was changed from 25G from 23G to account for the difference in the viscosity of new PCL-HA slurry.

Segmental Defect Dogs 5 and 6 received canine allografts (Veterinary Transplant Services, Kent, WA) instead of scaffolds. The surgeries and follow-up testing were performed in exactly the same manner as the scaffold procedures.

Segmental Defect Dogs 8, 9 and 10 received sterilized scaffolds seeded with 2.5 mg of BMP-2 protein microspheres. BMP-2 microspheres were synthesized with BMP-2 protein encapsulated into poly(DL-lactic-*co*-glycolic acid) (PLGA) microspheres through a [water-in-oil]-in-water double-emulsion procedure previously used by the co-PI of this grant (3). The microsphere loading procedure incorporated a specified amount of hydrophobic microsphere powder suspended in pure ethanol followed by immersing the scaffold into the ethanol loaded with the microspheres and mixing for 20 minutes. The liquid soaked scaffolds were then placed on glass, and sprayed with the ethanol plus microspheres suspension. The scaffolds were air dried, followed by gas sterilization. The scaffolds with BMP-2 microspheres had the same apparent strength and a similar physical appearance as the unseeded scaffolds.

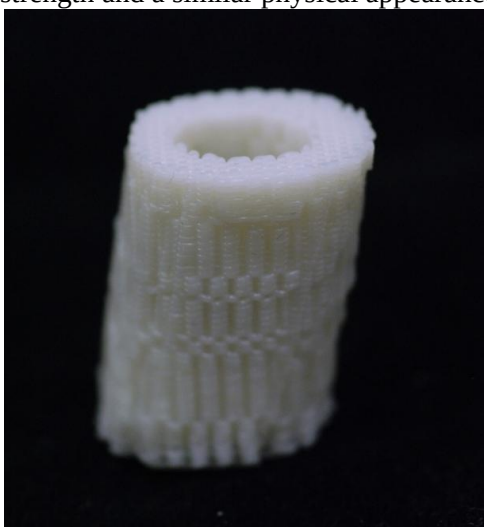

Figure 17: Photograph of 2 cm segmental defect scaffold showing no cortical shell and an 8 mm lumen.

2.2.2 Segmental Defect Surgeries

Segmental defect surgeries were done in accordance to the approved IACUC protocol as detailed in the 2012 annual report. For the Segmental Defect Dogs 1 through 7, a 3.5-mm-8-hole locking compression plate (LCP) system from the Synthes® veterinary division (West Chester, PA) was used. Dogs 3 and 7 experienced plate bending and were sacrificed early. To avoid this problem, a 3.5 mm-8-hole locking compression plate was tested (Section 2.2.3) and used for Dogs 8, 9 and 10. To date, these dogs have no evidence of plate bending. Figure 18 shows the placement of the unseeded scaffold in Dog 4. Figure 19 shows the allograft placement in Dogs 5 and 6. Figure 20 is an intra-operative view of the unseeded scaffold placement in Dog 7, and the subsequent failure of the plate at Post-op Day 35. Figure 21 shows the placement of the BMP-seeded scaffold for Dogs 8, 9 and 10.

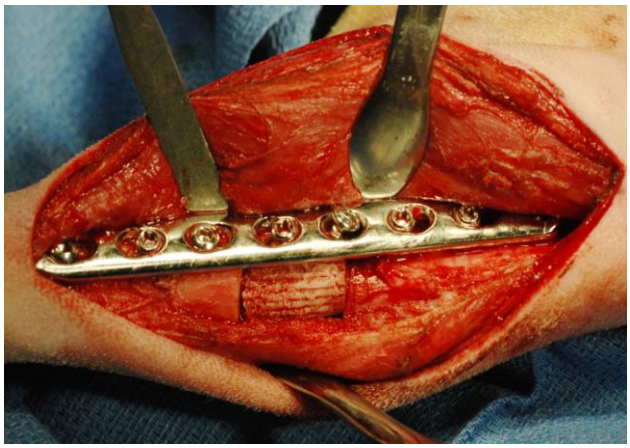

Figure 18: Segmental Defect Dog 4, right tibia with scaffold implant during surgery.

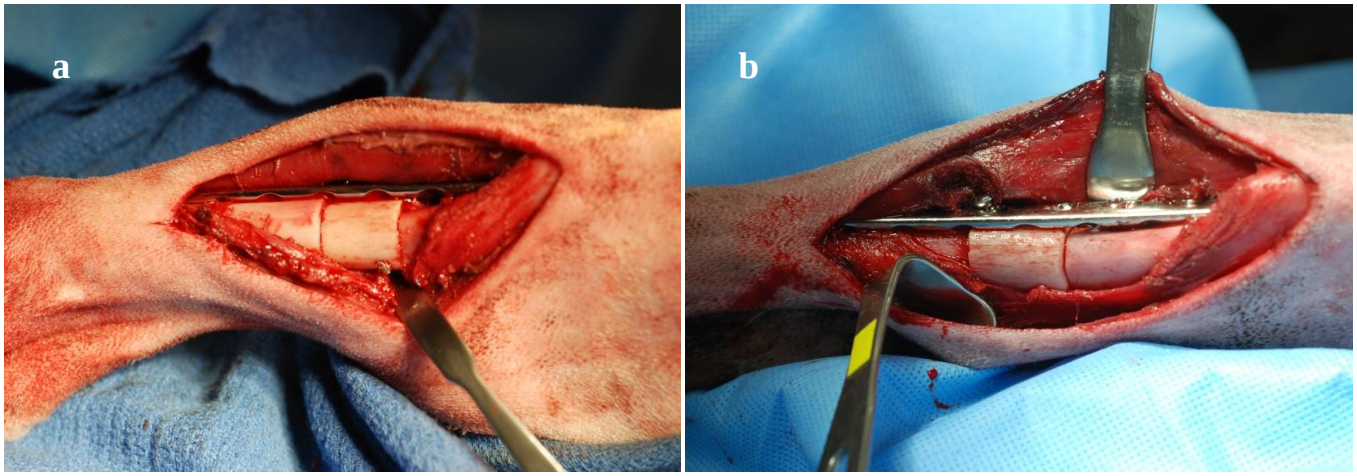

Figure 19: Operative photo showing sterile field, LCP plate and placement of dog cadaveric allograft in segmental defect in the exposed lateral side of right hind tibia of Segmental Defect (a) Dog 5 and (b) Dog 6.

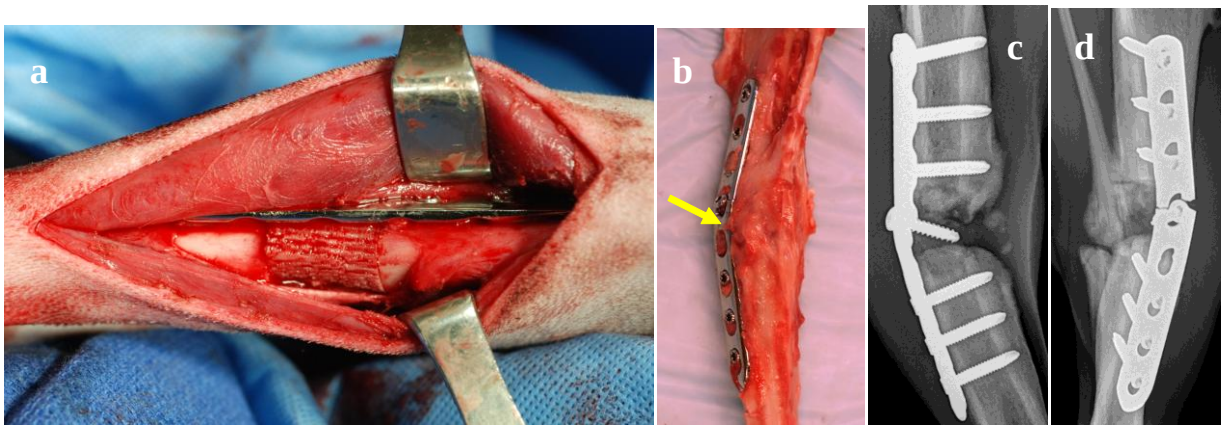

Figure 20: Segmental Defect Dog 7 right tibia (a) scaffold implant during surgery, (b) photo after sacrifice showing bent plate with arrow denoting breaking point, radiograph at Post-op Day 35 of bent plate prior to dissection in (c) anterior-posterior view and (d) media view.

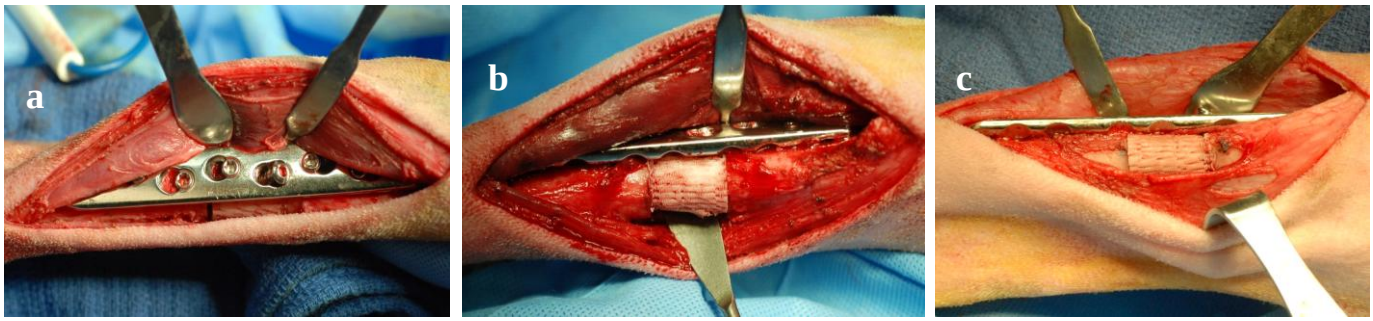

Figure 21: Operative photo showing sterile field, intensified and broad LCP plate and placement of BMP-2 microsphere attached scaffold in segmental defect in the exposed lateral side of right hind tibia of Segmental Defect (a) Dog 8 (b) Dog 9, (c) Dog 10.

Segmental defect Dog 4 received a scaffold implant surgery and experienced no post-surgery problems. However, Dog 7 experienced an adverse event. The dog appeared to be recovering as expected after surgery, with moderate weight bearing on the operated limb. On Post-op Day 14, the routine radiographs showed bone healing. This dog appeared to be

physically healthy and recovering well with moderate weight bearing. The dog was allowed a limited routine daily exercise under direct supervision of the ICM veterinary technician. On June 20 (Post-op Day 30), the routine radiograph revealed a slight lateral bending of the fixating plate at the mid-point, and a fibular fracture at the defect level. The daily activity level was restricted to a 15-minute leashed exercise twice a day by a veterinary technician. On June 23, the dog appeared to be experiencing moderate pain involving the right hind leg, with minimal weight bearing. On June 24 (Post-op Day 34), the dog was sedated and a series of implant site radiographs were obtained. The images revealed increased bending of the fixating plate with integrity failure at the mid-point and fibular fracture. The dog was euthanized while under sedation, at the advice of the ICM veterinarian. The post-mortem right hind leg exam showed a plate failure and moderate lateral deviation of the distal limb. No other gross abnormalities were found during the necropsy exam by the ICM veterinarian.

Dogs 5 and 6, with allograft implants underwent their full 16 weeks post-surgery recovery period and then were humanely sacrificed and both hind limbs removed by disarticulating the hip. The tibiae were then carefully excised and all soft tissue removed in preparation for biomechanical testing. The fibulae of both experimental (right limbs) were found to be adhered to the tibia in the immediate vicinity of the plate via callus formation. Using sharp dissection and where necessary, a small oscillating power saw, the adhered fibulae were carefully removed without damaging or putting undue stress on the tibiae. There was callus formation around the edges of the plate and in the screw holes of the plate for all three dogs as shown Figure 22. All locking screws were found to be tight upon removal. The cortical screws in each allograft were not loose, nor were they tight. They had not backed out, maintaining the same position on the plate as during initial insertion.

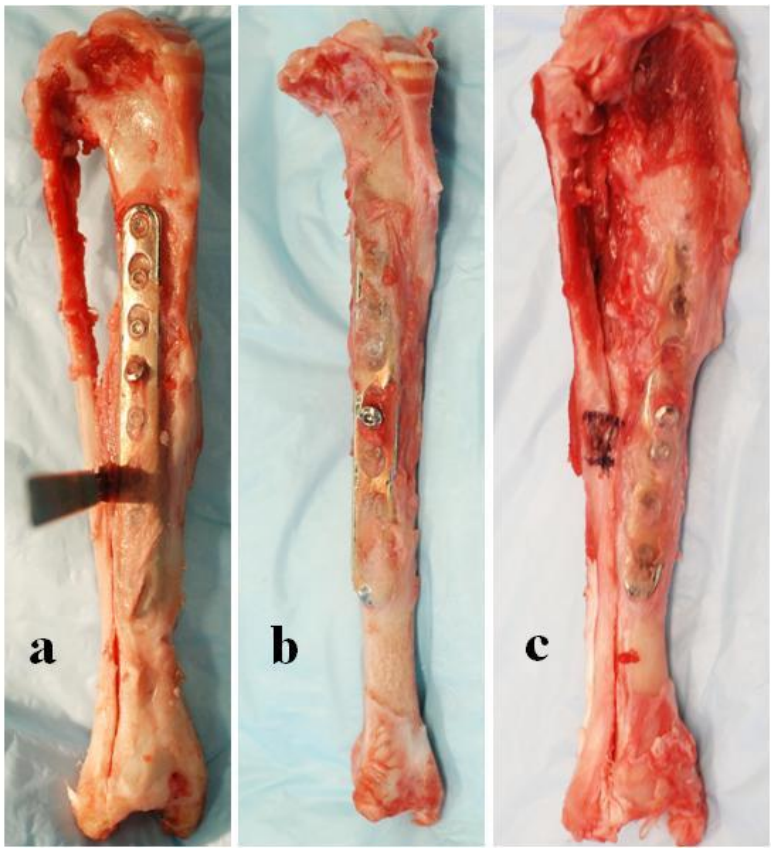

Figure 22: Lateral view of dissected tibiae of (a) Segmental Defect Dog 4 (unseeded scaffold), (b) Segmental Defect Dog 5 (allograft) without fibula attached, and (c) Segmental Defect Dog 6 (allograft).

2.2.3 Comparison of Standard and Broad LCP Plates in Response to Adverse Event

The response to the plate bending for Segmental Defect Dog 7 was reported to the DOD in an email dated July 17th and is provided in part below.

The event occurred on June 24, 2013. The adverse event report (attached) was filed with the Columbia IACUC on July 15, 2013. Prior to submission of the report, a careful dissection of the affected limb was performed to understand the cause of the event and laboratory mechanical testing was conducted to suggest

corrective action. Based on the X-rays prior to sacrifice and following dissection it was clear that the cause of the problem was plate failure due to bending. To rectify this problem, the use of a stiffer, stronger mending plate was proposed.

To test this hypothesis, we compared the plate we have been using with a slightly wider and thicker plate. To date we have used a 3.5 mm screw size LCP plate that is 11.0 mm wide and 3.3 mm thick. A 3.5 mm screw size LCP-Broad plate is available from the Synthes Vet division, the manufacturer from which we have obtained our standard LCP plates. The LCP-Broad plate is 13.5 mm wide and 4.2 mm thick. The bending stiffness of a flat plate is proportional to the 3rd power of the thickness and linearly to the width. Hence, increasing the thickness of the plate by 0.7mm and the width by 3.5 mm increases the bending stiffness by approximately 250%.

To verify this increase in stiffness, mechanical tests were performed on 2 right tibiae from 2 of the osteochondral dogs of approximately the same size that had been saved in the freezer following harvesting of the femora as per the Aim 1 of this project. A broad LCP plate was used on one tibia and the standard LCP plate that we have been using to date was used on the other limb. After plating, 1000 cycles of axial load were first applied to mimic the dog undergoing normal ambulation, using numbers from the canine gait analysis literature. A ramp load was applied, lateral to medial, as shown in Figure 23, to cause the plate to bend. As shown in Figure 24, the broad LCP plate / bone construct is significantly stronger than the LCP plate / bone construct. The bone broke off at the fixation point for the broad LCP plate exhibiting no bending when the bone failed. However, the LCP plate exhibited a great deal of bending at significantly lower loads. In summary, the broad LCP plate bone construct was found to be much stronger than the LCP plate bone construct that we have been using for the segmental (Aim 2) defect component of this study.

The proposed use of the 3.5 Broad LCP was presented to the Columbia IACUC in August of 2013 and was approved, as well as using 3.5 mm plugs in the used holes of the Broad Plate. These plates and plugs were used in Dogs 8, 9 and 10.

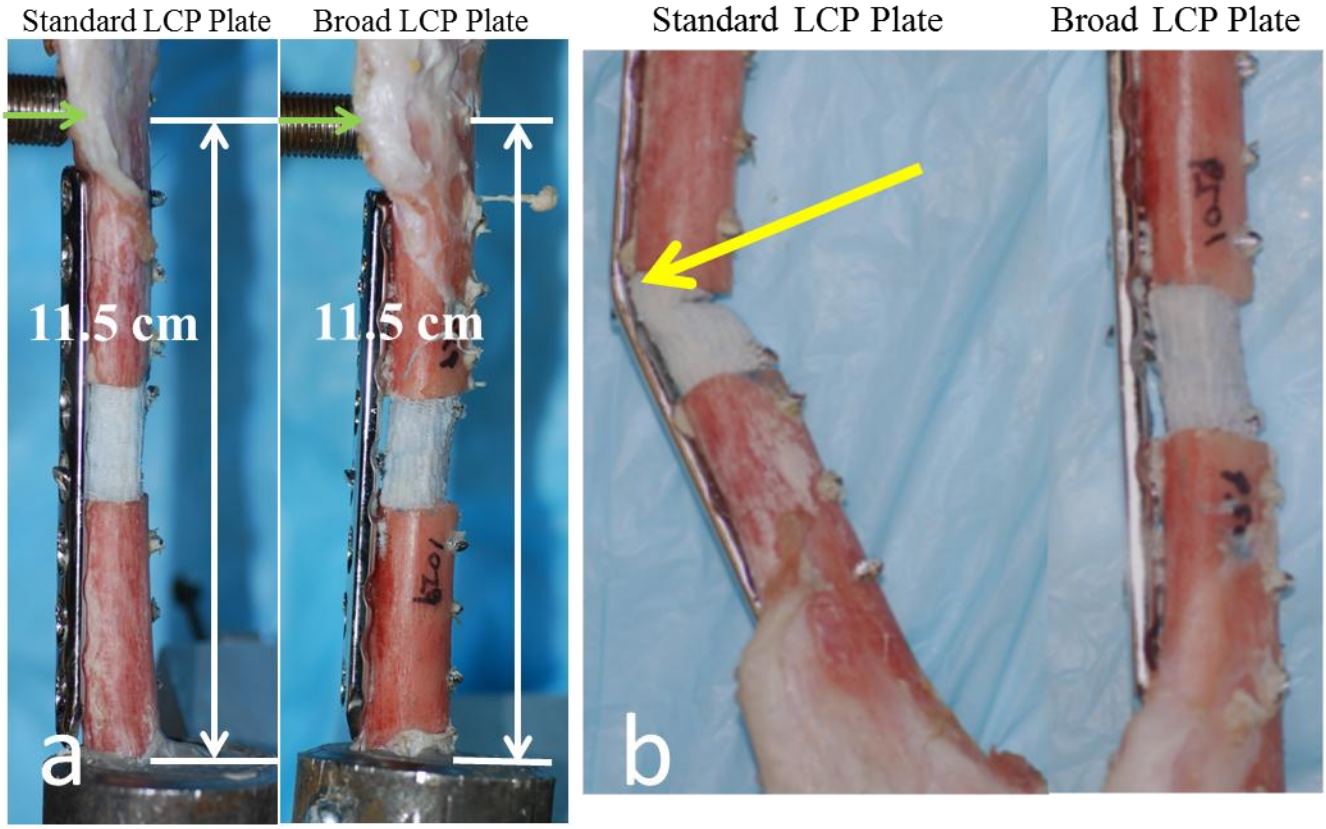

Figure 23: (a) Mechanical test set-up to compare Standard LCP and Broad LCP plates, green arrows denote direction of bending, (b) failure results showing bending of Standard LCP plate, denoted by yellow arrow, and unbent Broad LCP plate on the right.

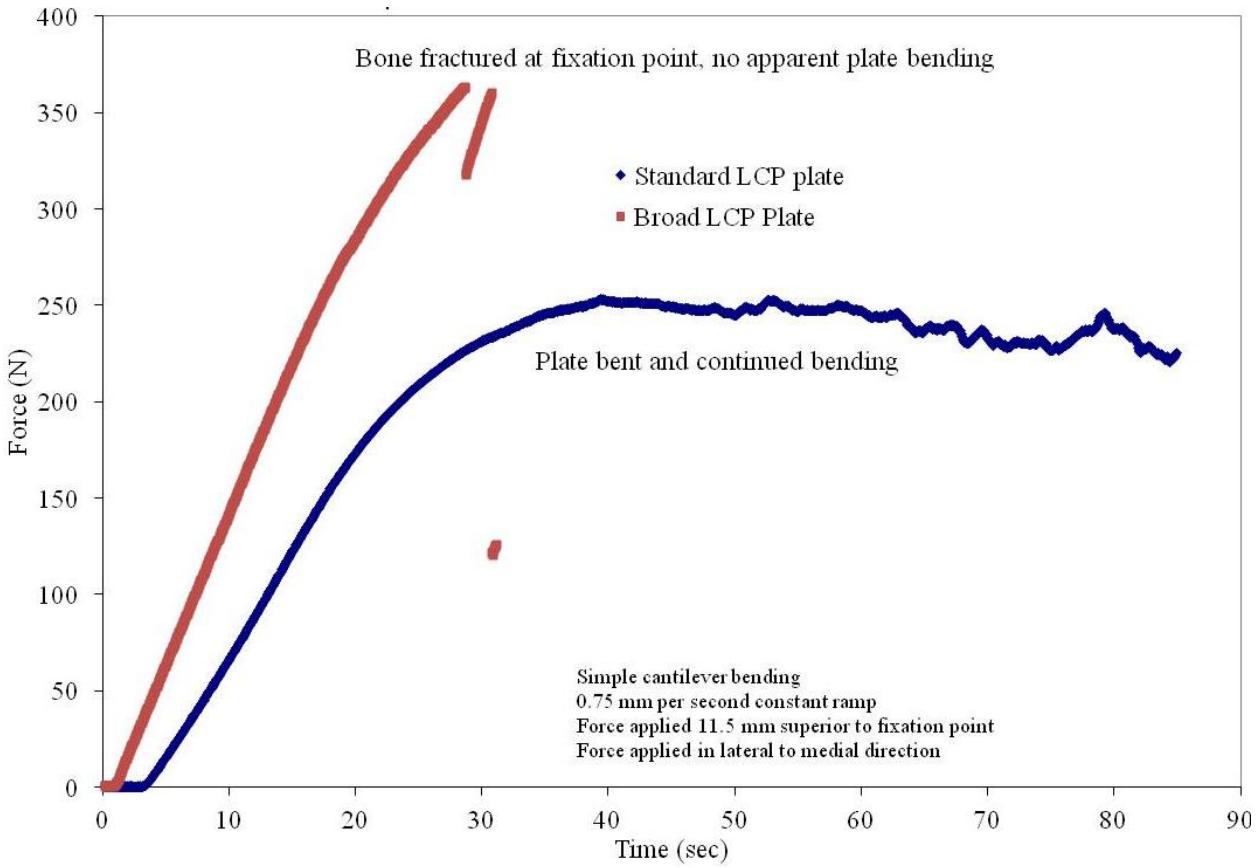

Figure 24: Failure bending results comparing Broad LCP plate to Standard LCP plate.

2.2.4 Segmental Defect Outcome Measures

Outcome measures of gait, lameness, pain, knee motion and an aggregate of these measures were recorded for each dog every weekday (refer to Table 1 for criteria), excluding Saturdays and Sundays. As can be seen from Figure 25 and Figure 26, Dog 4 and Dog 5 maintain a high total score immediately following surgery and throughout the entire 16 week period. Dog 6 (shown in Figure 27) had an initial period of more pain and lameness but these conditions improved by day 30 and remained similar to those of Dog 5 for the duration of the experimental period. The outcome graph of Dog 7 has a similar trend as Dog 5 and also maintains a high score level until Post-op Day 30 after which catastrophic failure of the plate occurred and the dog was sacrificed. The outcome measures for Dogs 8, 9 and 10 with the BMP-2 seeded scaffolds show good total scores by approximately day 15, which is somewhat earlier than that of the previous segmental defect dogs.

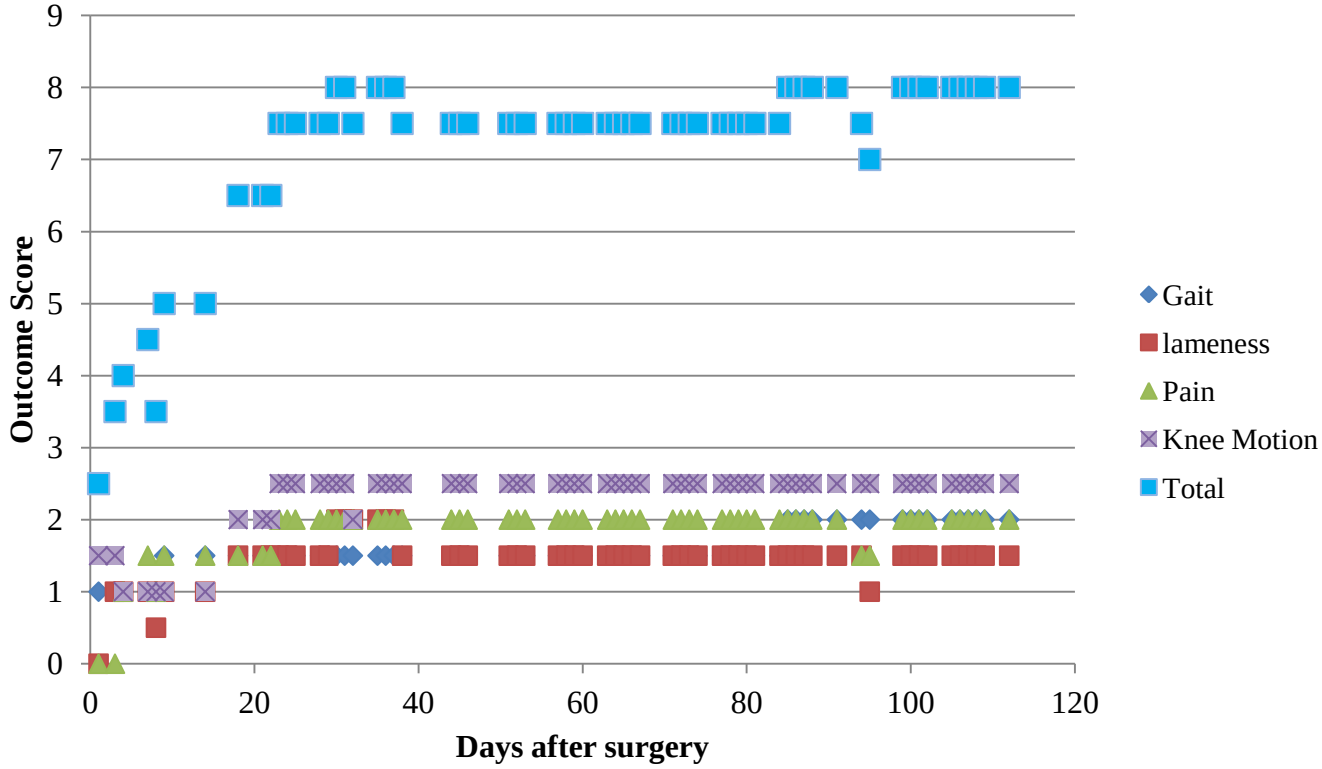

Figure 25: Outcome measurement for Segmental Defect Dog 4.

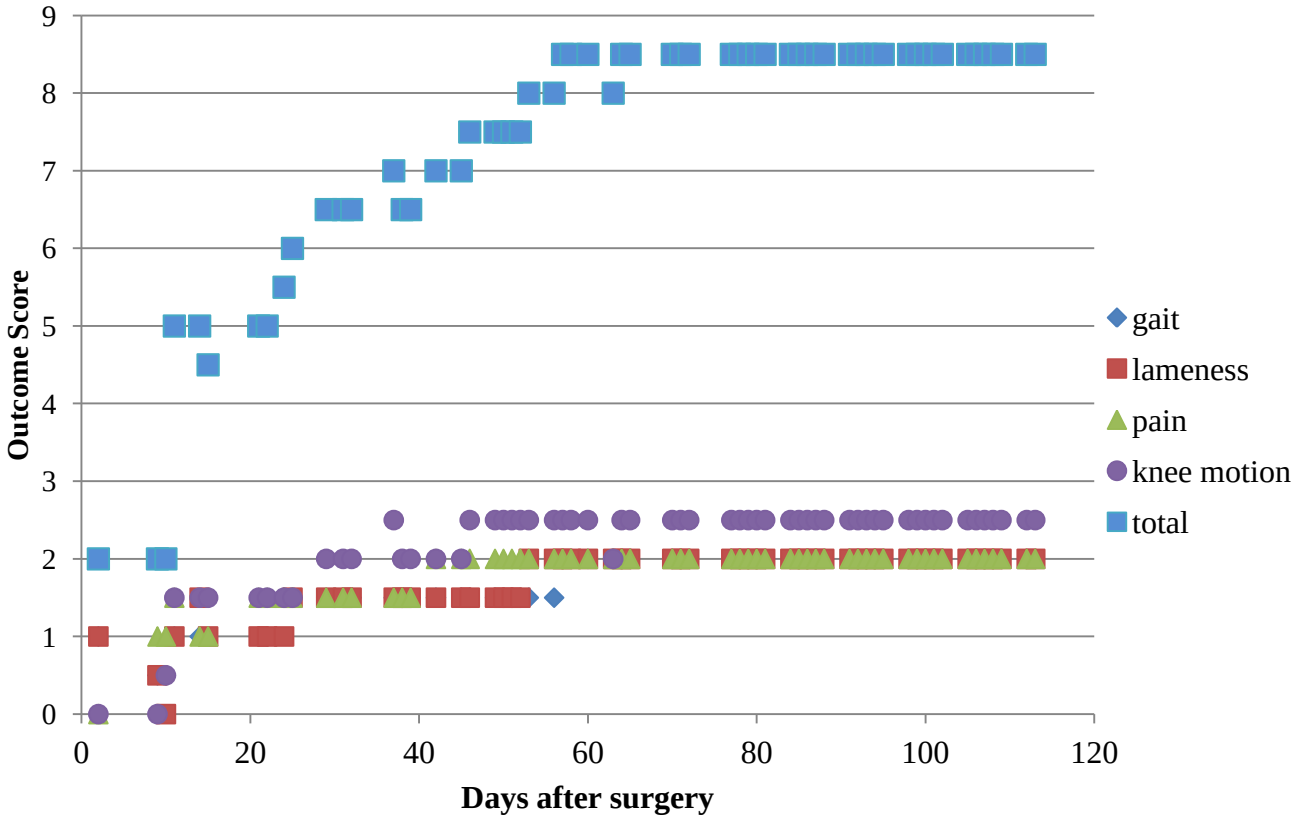

Figure 26: Outcome measurement for Segmental Defect Dog 5.

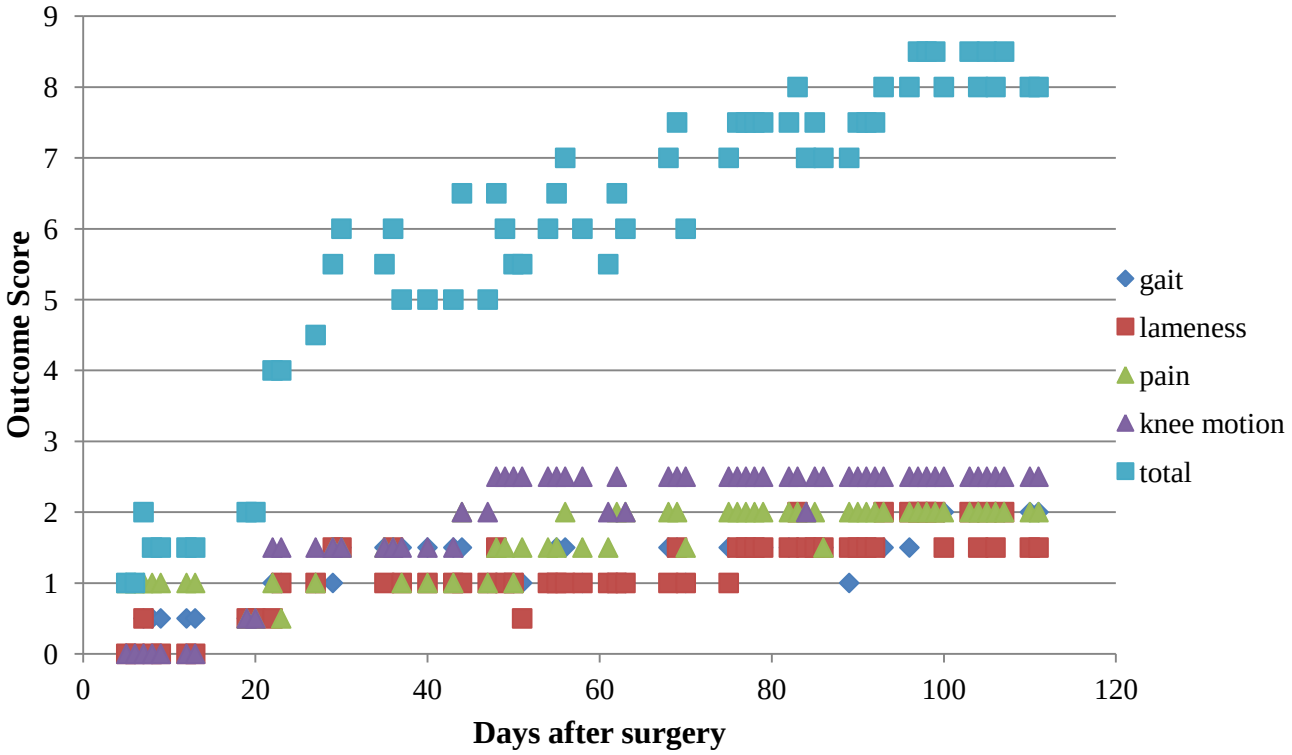

Figure 27: Outcome measurement for Segmental Defect Dog 6.

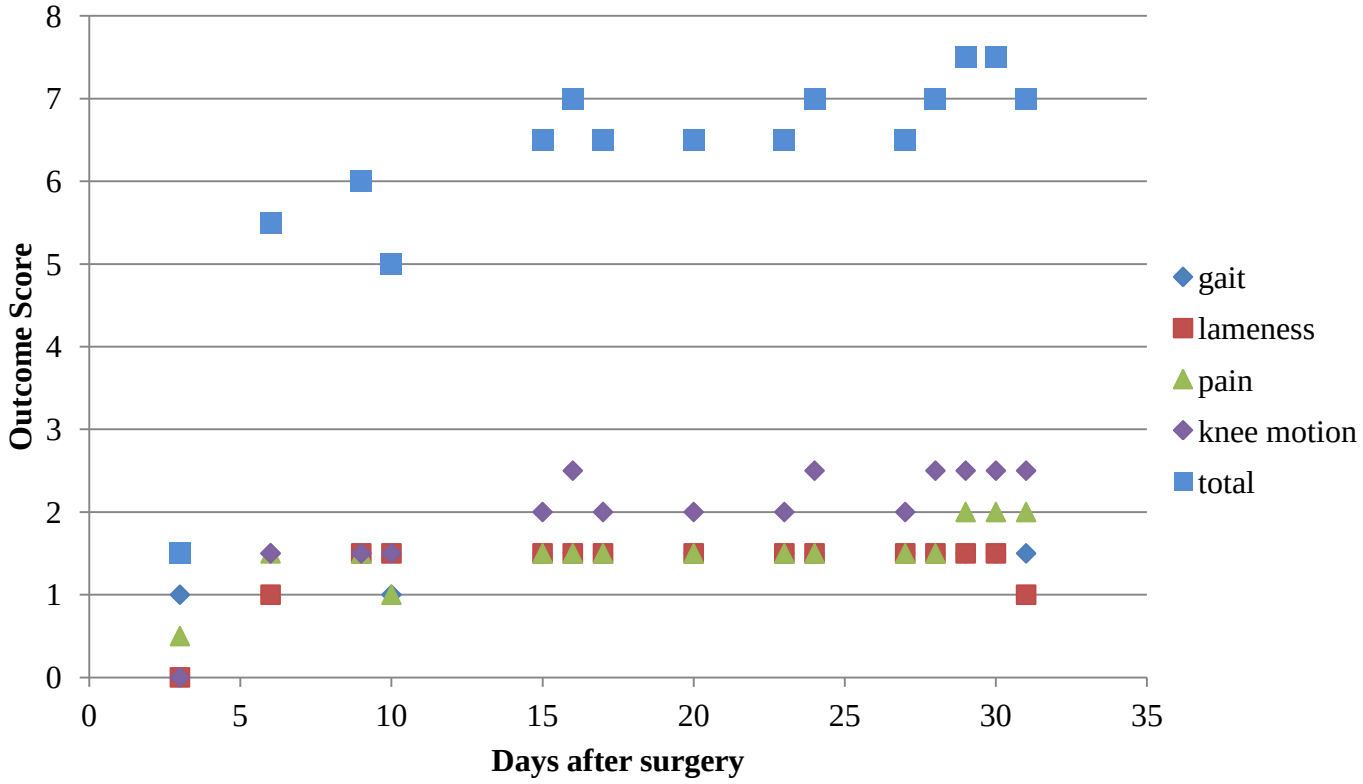

Figure 28: Outcome measurement for Segmental Defect Dog 7.

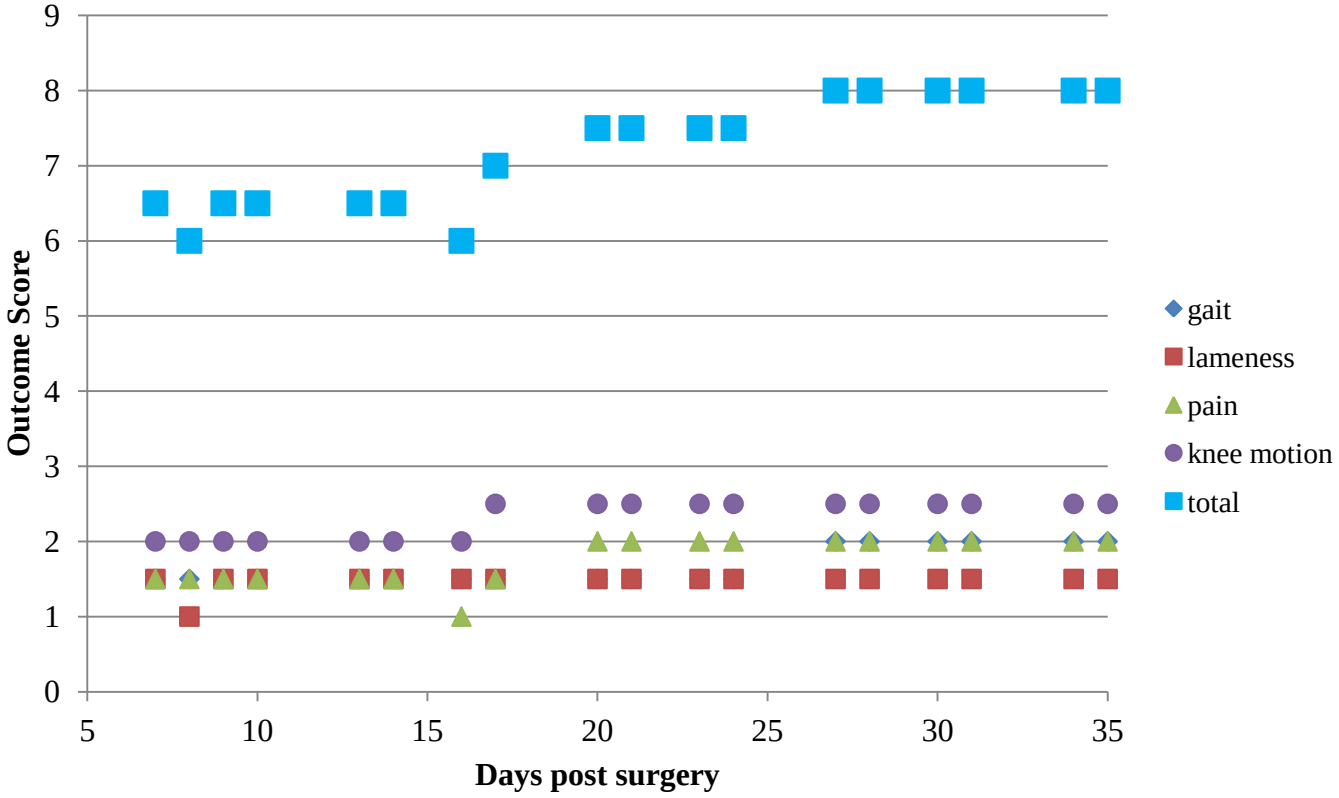

Figure 29: Outcome measurement for Segmental Defect Dog 8 until Post-OP Day 35.

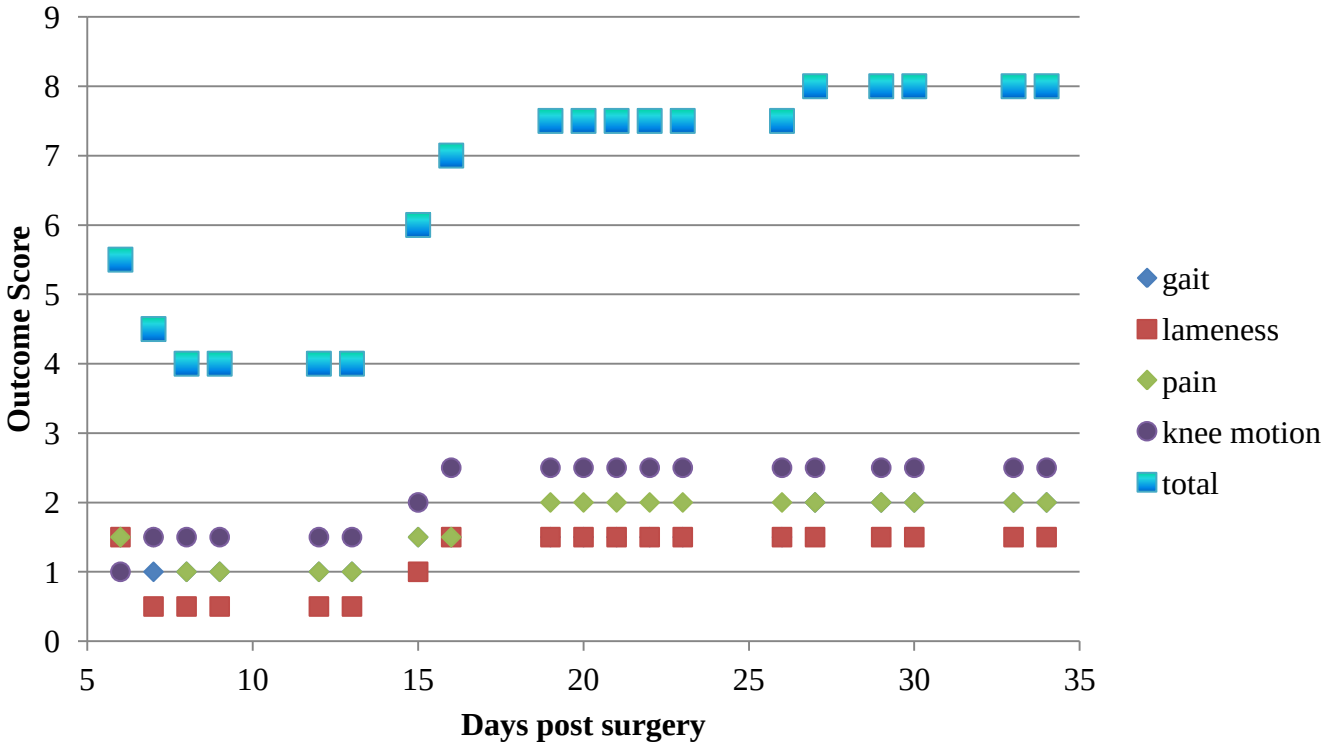

Figure 30: Outcome measurement for Segmental Defect Dog 9 until Post-OP Day 34.

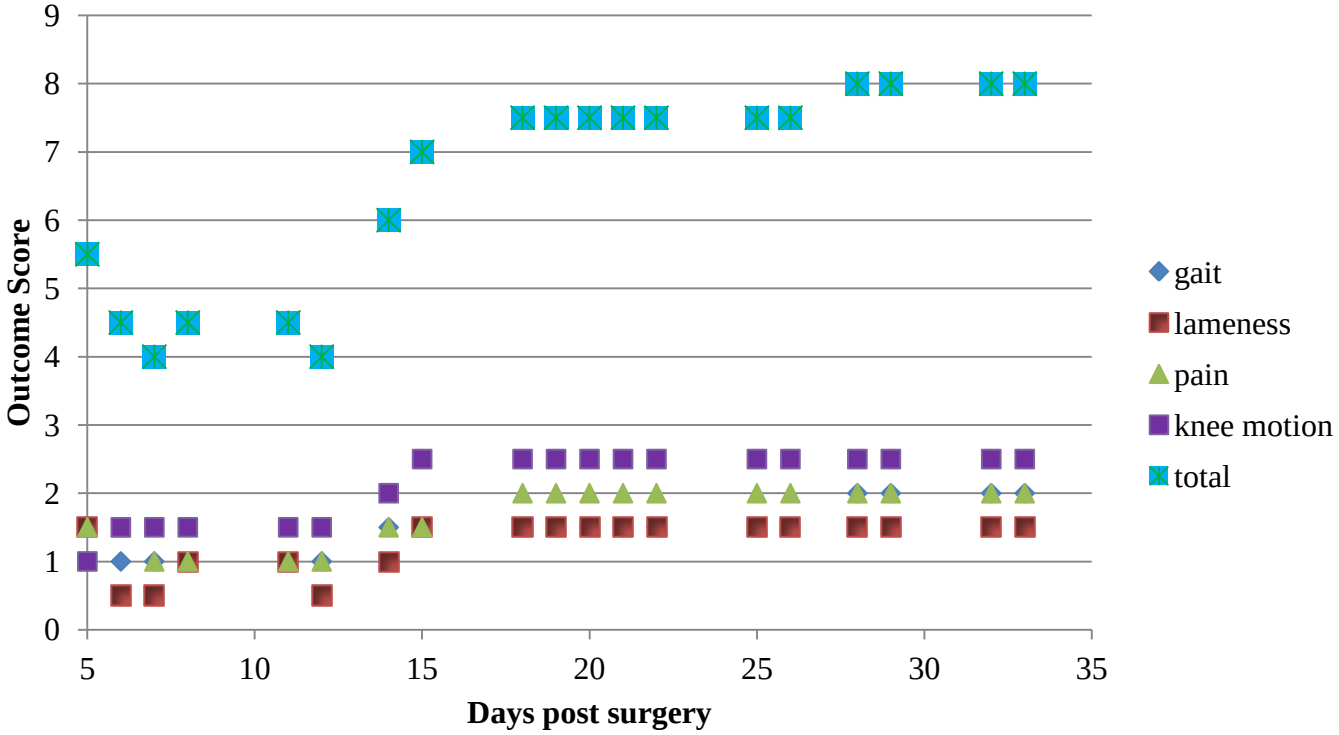

Figure 31: Outcome measurement for Segmental Defect Dog 10 until Post-OP Day 33.

2.2.5 Segmental Defect Radiographs and 3-D Models from CT Imaging

Digital radiographs were taken of all segmental defect dogs every two to four weeks. Figure 32 shows the progression of healing for Segmental Defect Dog 4. Little callus formation is seen until post-op week 4. By week 8, the bony ingrowth into the lumen of the scaffold is clearly seen. The callus covering the scaffold reaches its maximum volume in Week 8 and then decreases. The 3-D computer model for CT images for Dog 4, Figure 37, shows the volume of callus in the middle of the tibia, and bony ingrowth into the lumen of the scaffold for Dog 4 is not well-distinguished. Figure 33 and Figure 34 show the radiographic time history of Segmental Defect Dog 5 and Dog 6 that received cadaveric canine allografts. For these two dogs, slight callus formation can be seen by post-op week 2 and progresses significantly until week 8, after which it keeps growing gradually until sacrifice. Meanwhile the gaps between the allograft and the superior and inferior tibial surfaces appear to begin fusing after post-op week 8. As can be seen from the 3-D computer models created for the CT images for Dog 5 and Dog 6, Figure 38 and 39, respectively, callus covers the allografts by post-op week 8.

The radiographs for Dog 7 in Figure 35 show slight plate bending by week 2 PO and catastrophic plate failure at Post-op week 5. The initial radiographs for the Dog 8, 9 and 10 of the recent September surgeries with BMP-2 seeded scaffolds, Figure 36, show maintenance of fixation with little ingrowth at this time.

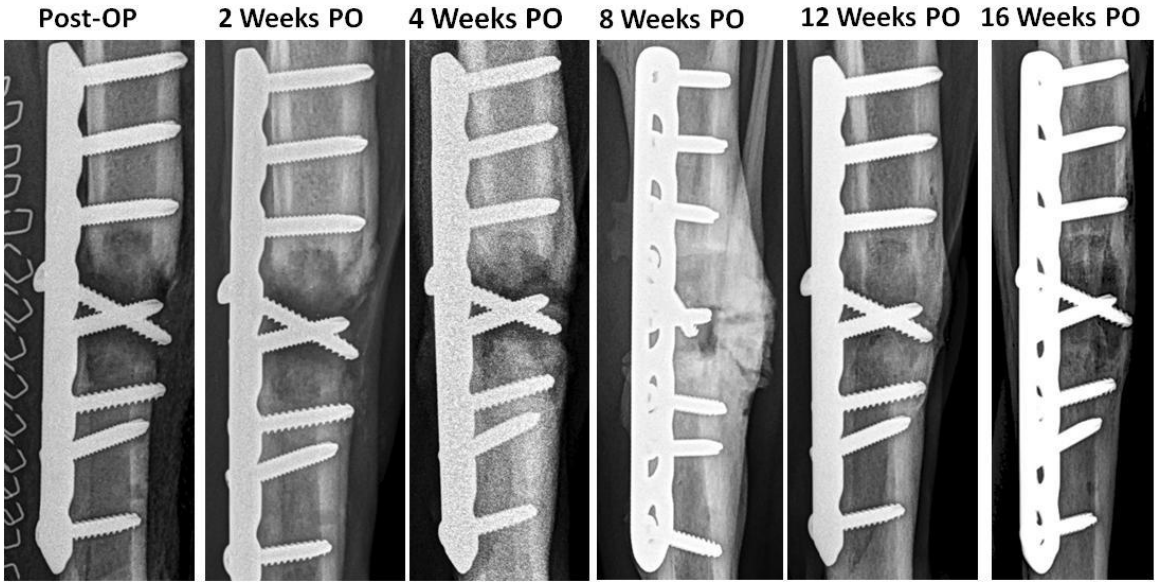

Figure 32: Radiograph of lateral view for Segmental Defect Dog 4 (unseeded scaffold) as a function of time showing the progression of callus formation in the vicinity of the scaffold (relatively dark area with oblique screw through it).

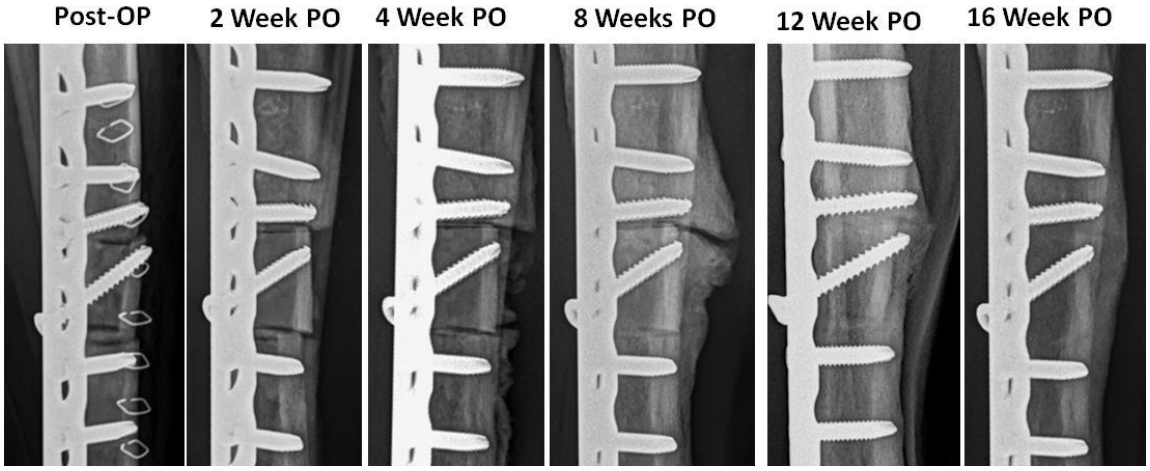

Figure 33: Radiograph of lateral view for Segmental Defect Dog 5 (allograft) as a function of time showing progress of callus formation in the vicinity of the allograft (the area between the two cuts with an oblique screw). By post-op week 8 the gaps between both superior and inferior ends of the allograft was clearly narrowing.

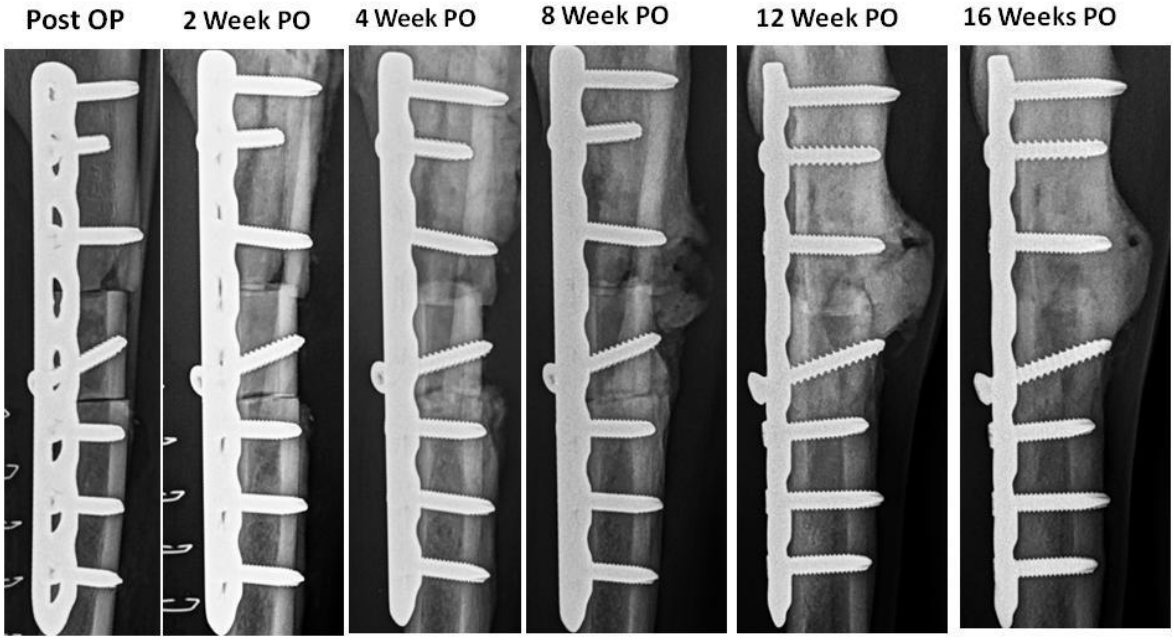

Figure 34: Radiograph of lateral view for Segmental Defect Dog 6 (allograft) as a function of time showing progress of callus formation in the vicinity of the allograft (the area between the two cuts with an oblique screw). As for Dog 5, by post-op week 8 the gaps between both superior and inferior ends of the allograft was clearly narrowing

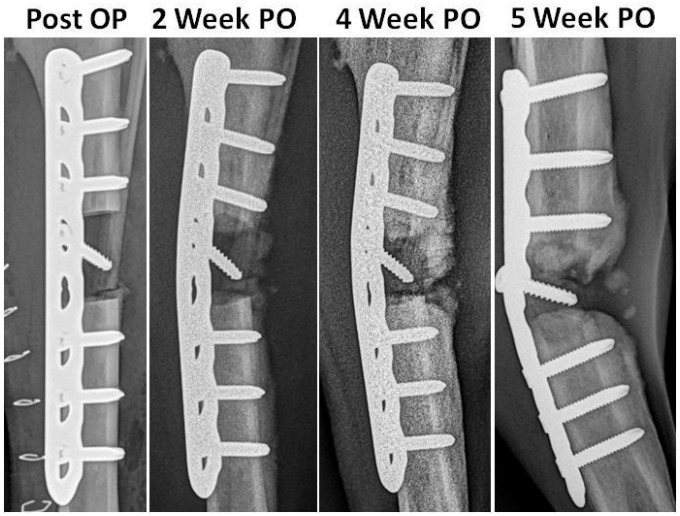

Figure 35: Radiograph of lateral view for Segmental Defect Dog 7 (unseeded scaffold) as a function of time showing. Slight bending of the plate is apparent by week 2, with catastrophic plate failure occurring at week 5 PO.

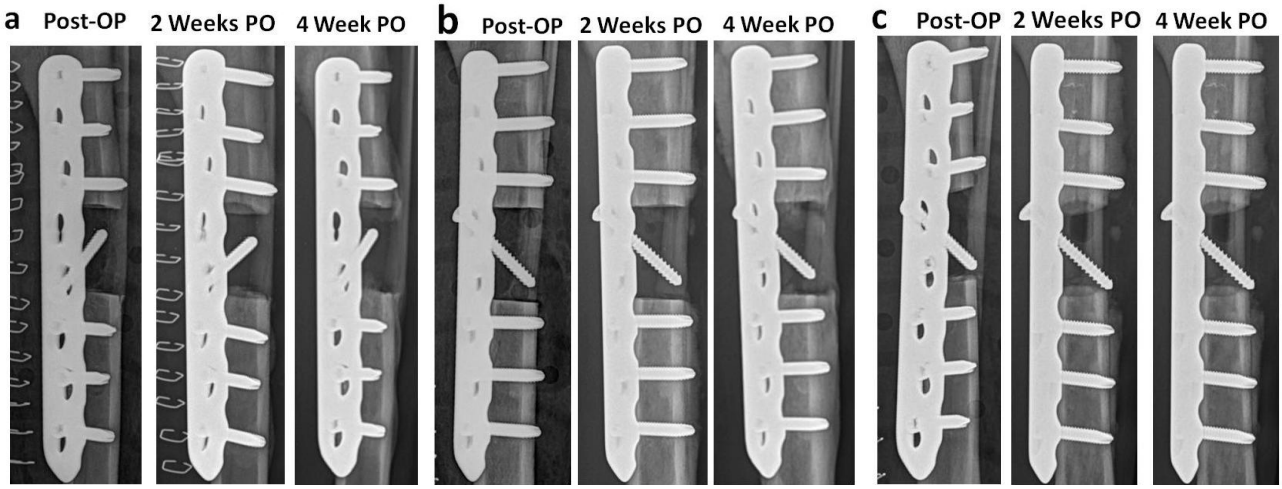

Figure 36: Early radiographs of lateral view for (a) Segmental Defect Dog 8 (BMP-seeded scaffold), (b) Segmental Defect Dog 9 (BMP-seeded scaffold) and (c) Segmental Defect Dog 10 (BMP-seeded scaffold).

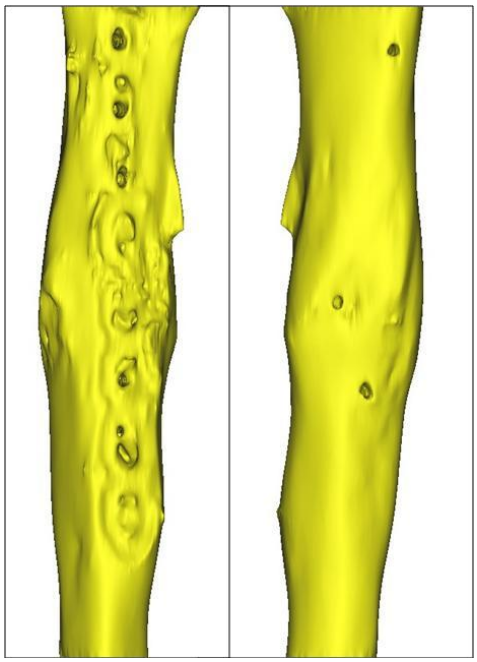
Figure 37: 3-D computer model of experimental right tibia of Segmental Defect Dog 4 (unseeded scaffold). Left is lateral-medial view of tibia and right is the posterior-anterior view.

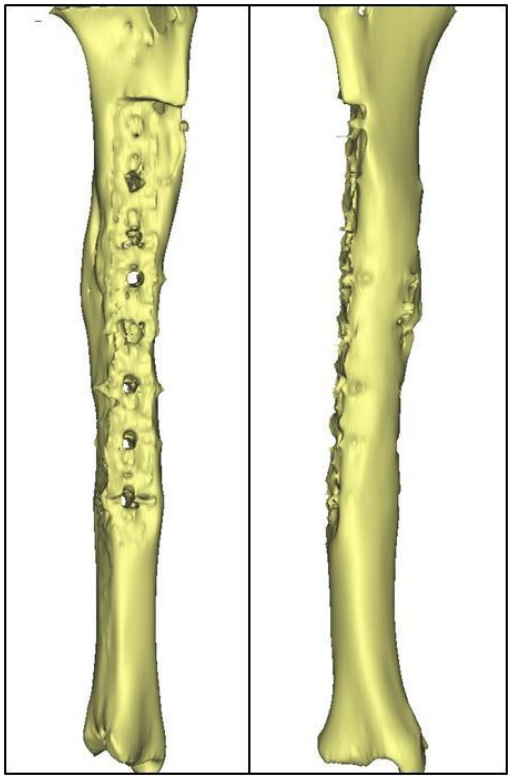

Figure 38: 3-D computer model of experimental right tibia of Segmental Defect Dog 5 (allograft). Left is lateral-medial view of tibia and right is posterior-anterior view.

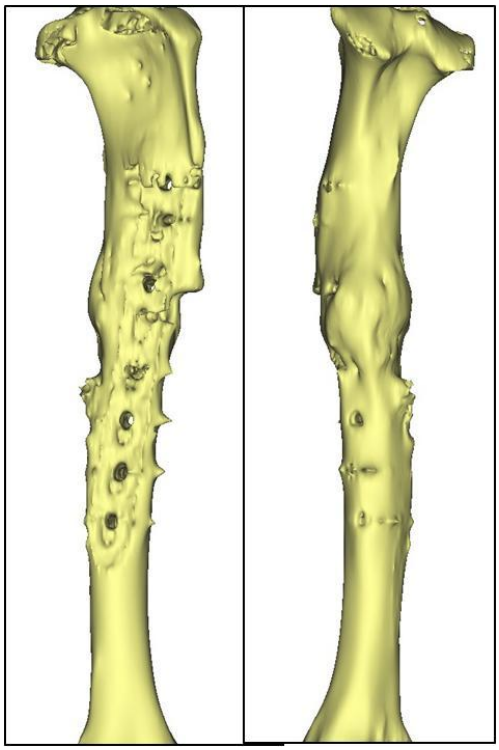

Figure 39: 3-D computer model of experimental right tibia of Segmental Defect Dog 6 (allograft). Left is lateral-medial view of tibia and right is posterior-anterior view.

2.2.6 Biomechanical Testing of the Segmental Defect Dogs

Mechanical testing in axial compression with the plate attached followed by torsion in internal rotation until failure were performed for Segmental Defect Dogs 4, 5 and 6 as detailed in the 2012 Annual Report. Dog 7 was not tested because it was sacrificed early due to catastrophic plate failure. Table 2 provides the failure results for these dogs, as well as for the second dog tested, Dog 2 and reported last year. The values

for Dog 1, though tested were reported last year, but are not included here because it was apparent that it was broken during specimen preparation and will not be used in any statistical analyses moving forward.

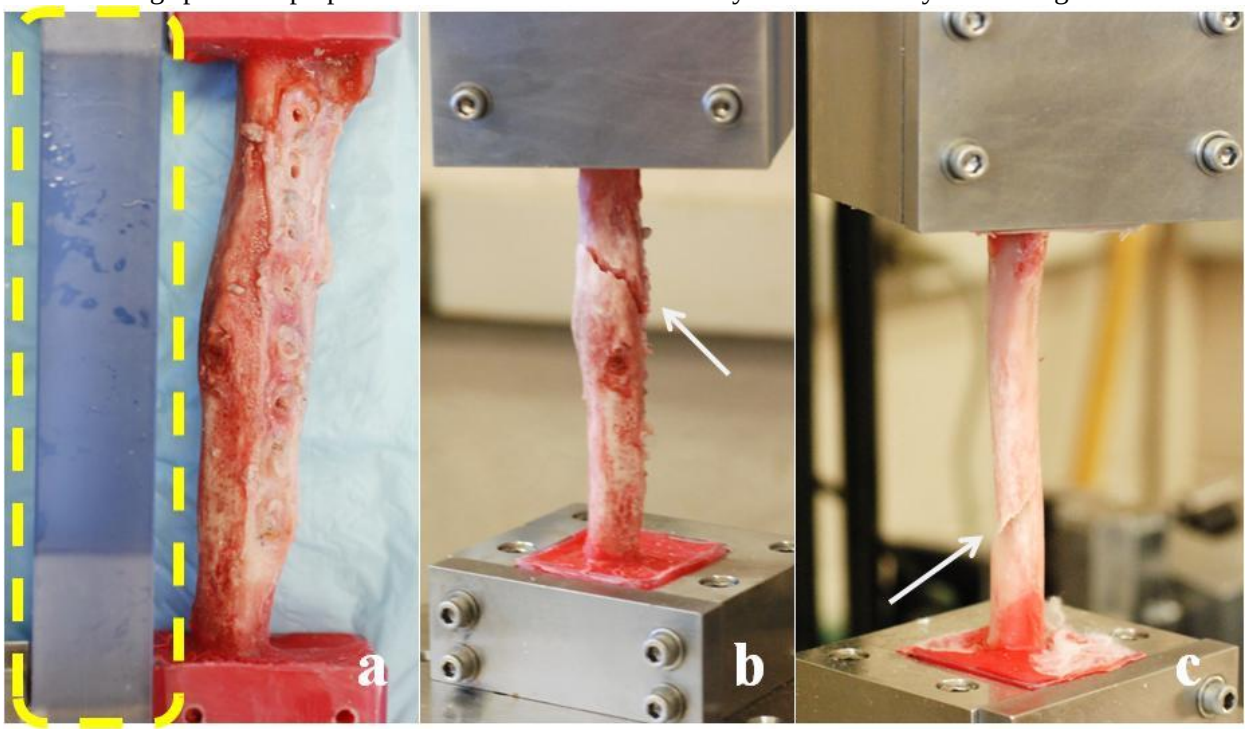

Figure 40: (a) The rigid polycarbonate support attached to the potted blocks to secure the tibia during removal of screws and plate is highlighted by the dashed region; biomechanical testing of the Segmental Defect canine tibiae (b) experimental tibia with hardware removed and (c) contralateral control tibia. Similar spiral fractures, denoted by arrows, are apparent on both tibiae.

Ratios of the biomechanical test parameters (experimental/control) in terms of percentage for failure torque, angular rotation at failure and rotational energy to failure are listed in Table 2. Neither the allograft nor scaffold implants fully restored the mechanical strength of the experimental limb to that of the control (non-operated) limb by the end of the 16 week recovery period. However, the mechanical results of the PCL-HA scaffolds for one dog were very comparable to that of the allograft dogs with the other scaffold dog somewhat lower, indicating that the PCL-HA scaffold can perform similarly to that of an allograft.

Animal	Failure Torque	Failure Angular Rotation	Rotational Energy to Failure
Dog 2 (Scaffold)	38.8%	63.1%	24.2%
Dog 4 (Scaffold)	80.1%	78.7%	65.7%
Dog 5 (Allograft)	67.1%	88.6%	61.9%
Dog 6 (Allograft)	82.3%	71.8%	55.7%

Table 2: Ratio of experimental tibia (right) to its contralateral control tibia (left) as a percentage for the experimentally measured values.

2.2.7 Segmental Defect Hard Sectioning Histology Study

Immediately following mechanical testing, the proximal and distal tibial potting blocks were cut off. The resulting diaphyseal portion of the tested bone was then soaked in 10% formalin solution for fixation for future histological evaluation. Because fixation for segmental specimens require more than two months, the tested specimens for Segmental Defect Dogs 4, 5 and 6 have not yet completed their fixation. The specimen for Dog 1 and Dog 2 that were sacrificed in 2012 have finished all preparation procedures for hard sectioning histology as described above in Section 2.1.6 and stained with H&E.

Figure 41(a) and 42(a) are of the entire mid-diaphysis of the tibia, including the scaffold and associated callus. The scaffold region can be distinguished from the region between the spiral screws marks at both ends and bony bone grow into most of the voids of PCL-HA scaffold and the lumen. The bone covering of the scaffolds is mostly cancellous bone, which can be clearly identified from Figure 41(c), and cartilage, which is apparently shown in Figure 42(c). Cancellous bone and cartilage are both present on the inside scaffold wall as shown in Figure 41(d) and 42(b). The hard section histological images of Segmental Defect Dog 1 and Dog 2 show the bony growth induction of the unseeded scaffold. In order to differentiate the bony growth from microscopic images, dynamic bone staining in live post-surgery dogs is highly recommended. A modification to the IACUC protocol to include this will be submitted shortly.

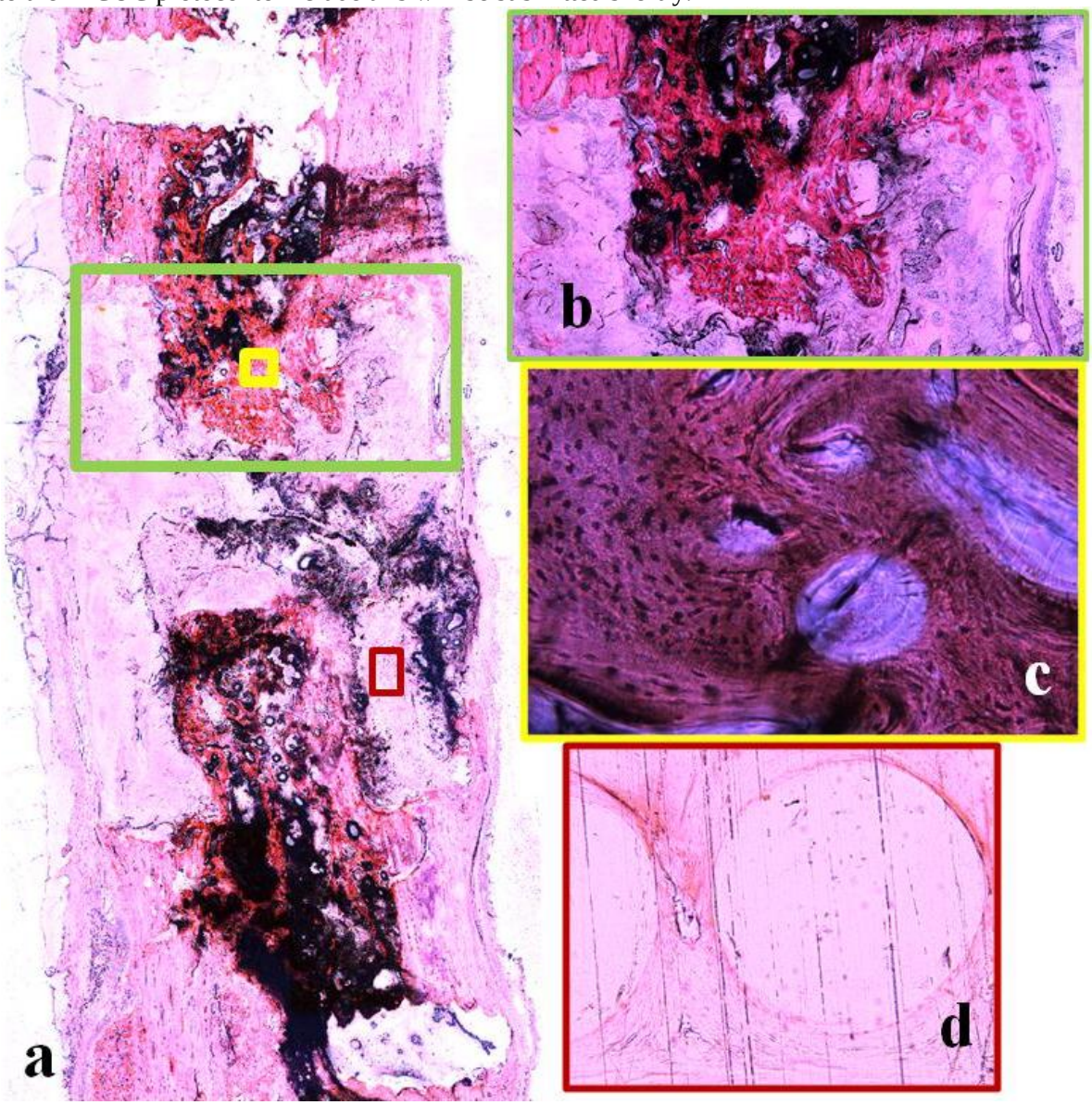

Figure 41: Hard sectioning histology image of Segmental Defect Dog 1, stained by H&E method. (a) Overview of middle right tibia with scaffold; the locking screws marks are the two blank regions both at the top and at the bottom of the image. (b) close-up of green rectangle region, the lumen region of the scaffold, (c) close-up of yellow rectangle region in 40X magnification, showing cancellous bone growth into the hole of the scaffold, (d) high magnification (20X) image of red rectangle region.

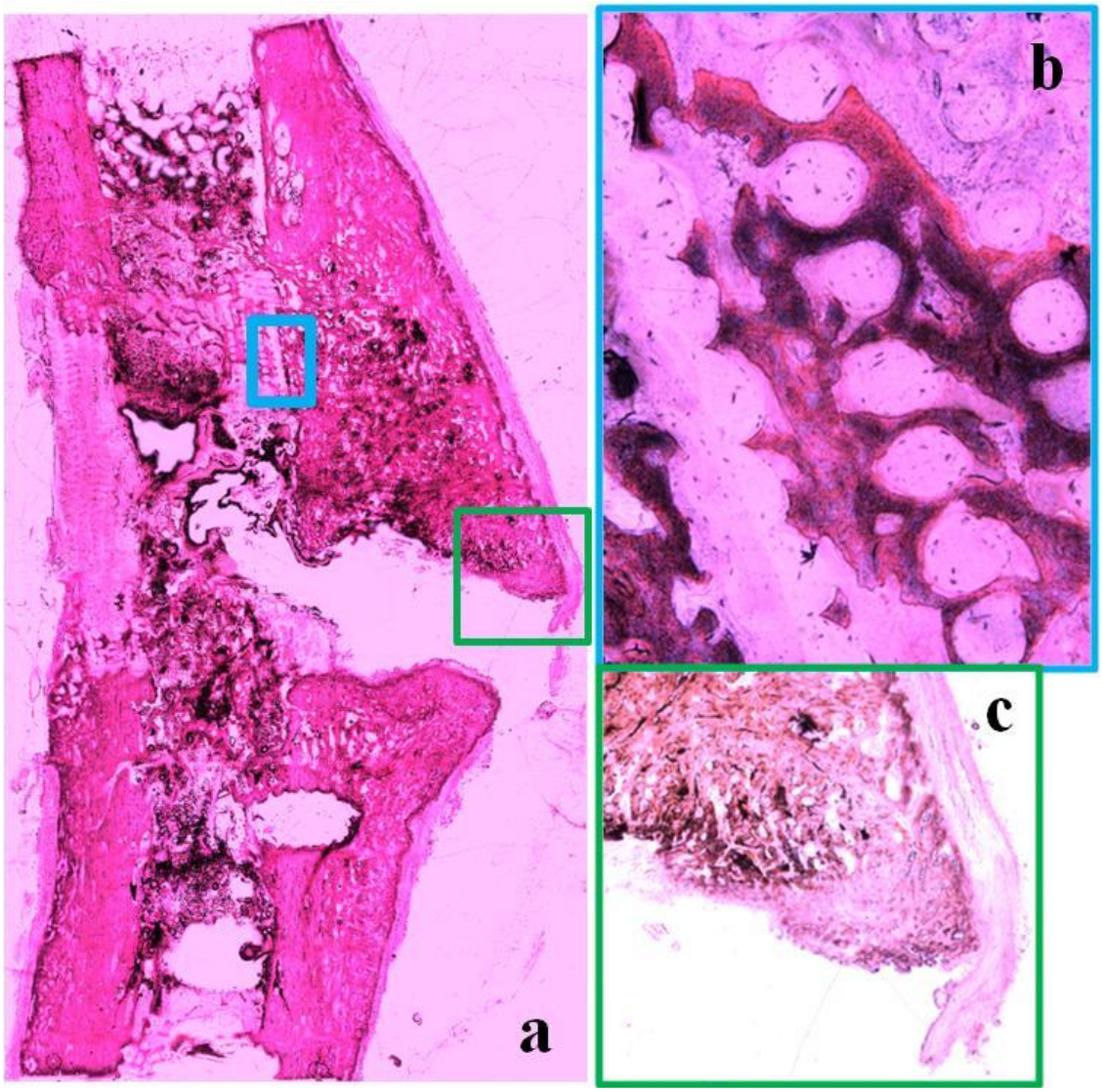

Figure 42: Hard sectioning histology image of Segmental Defect Dog 2, stained by H&E method. (a) Overview of middle of right tibia with scaffold, the locking screws marks are the two blank regions at the bottom of the image. (b) close-up of blue rectangle region, (c) close-up of green square region, cartilage covers the external surface of the cancellous bone. The discontinuation in the right side of the bone is due to the torsional fracture from biomechanical testing.

2.3 Aim 3 – Human Cadaveric Testing

Human cadaveric testing is provided for in the grant to assess the stability of the scaffold at time zero for both Aim 1 (osteochondral defects) and Aim 2 (segmental defects). All human cadaveric testing in support of Aim 2 has been completed.

2.3.1 Mounting of Plate in Human Cadaveric Tibia

Twelve human cadaveric tibiae specimens were used for this study. A medial incision was made and the soft tissue was sharply dissected down to the bone. The surrounding soft tissue and fibula were maintained to ensure that when the approximately 5 cm segmental defect was created, the native length of the tibia would be maintained. A 14-hole 4.5 mm broad, 260 mm long locking compression plate from Synthes (Paoli, PA) was used with five 5.0 mm diameter locking screws placed both superior and inferior to the scaffold. Two 4.5 mm diameter cortical screws were placed into the scaffold to secure it. Prior to placement of the cortical screws, two sutures were placed around the scaffold to hold it tightly to the plate as the screws were applied. All screws bridged both cortices. The scaffold was created using a mixture of 90% poly-caprolactone (PCL) and 10% hydroxyapatite (HA) by weight. The scaffold was created with 500 μm microchannels with 300 μm strands and did not have a cortex shell to replicate the scaffold architecture implanted in the dog. Figure 43 compares the implanted scaffold to the segment of bone removed from the tibia and its placement in the segmental defect. This will mimic the lateral approach that was used for segmental defect surgeries in the dogs.

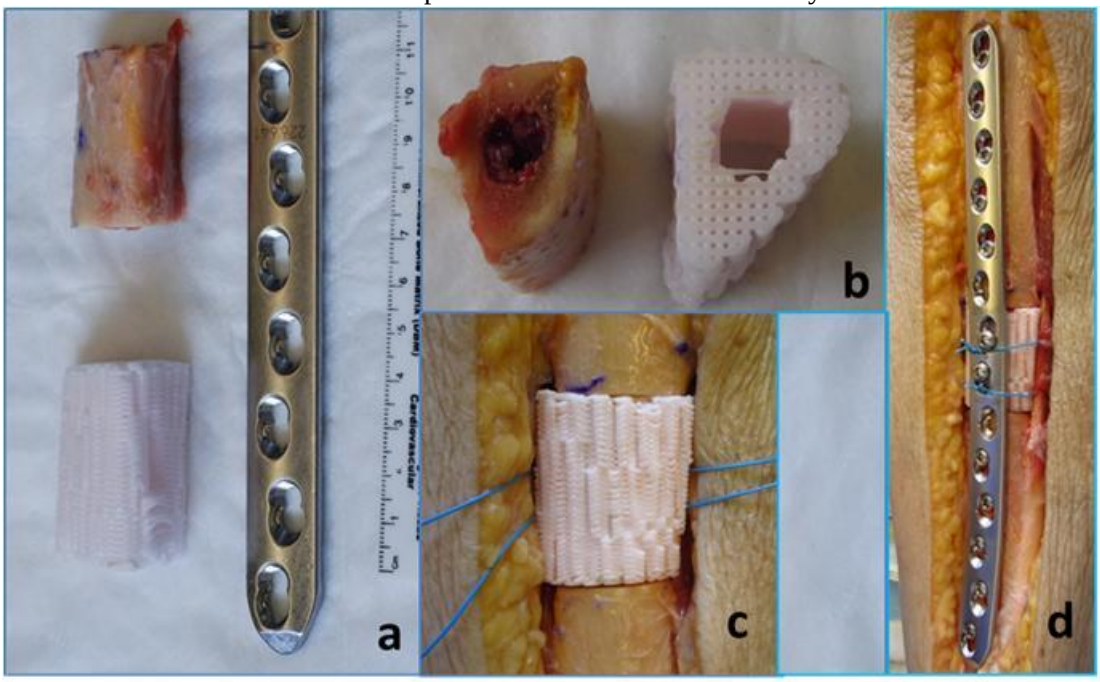

Figure 43: Human cadaveric tibial specimen showing a) excised segmental defect and scaffold to replace it, b) cross-sectional view showing human bone segment removed and scaffold, c) implanted scaffold showing tight-fit, d) locking plate, scaffold and bone construct.

2.3.2 Mechanical Testing of Human Cadaveric Tibia

The tibial plateau was first prepared by cutting off the raised portions to create a flat surface. Both the superior and inferior ends of the tibia were placed in polycarbonate square tubes. For torsional stability, two orthogonal 2.6 mm Steinmann pins were drilled through the tube and the tube-bone-pin construct was filled with PMMA. A metal plate was placed on the superior tube for axial loading via a steel ball was placed into the spherical depression in the plate and the tibia was loaded via a flat platen (Figure 44(a)). When torsion loading was to be applied, the ball was removed and the square tube, coated with grease to prevent axial loading, was placed into the square clamp (Figure 44(b)). The square superior clamp allowed the key to slide in the axial direction to permit superior/inferior motion of the plate as the tibia was torqued to minimize any compressive force resulting from the applied torque. The distal end of the tibia was potted in a similar manner and rigidly secured into a rigid square clamp at the base of the machine.

The loading was applied using a MTS 858 Bionix (MTS Eden Prairie, MN) testing system. Axial loading was applied via a series of step loads of 50 N, 400 N, 500 N, 600 N and 700 N. At each step, the load was applied in a sinusoidal fashion for 50 cycles at a rate of 2 Hz. Data were collected at a rate of 10 Hz. Bending loads were applied to the middle of the plate also via a series of step loads of 50 N, 200 N, 250 N, 300 N and 350 N in the same manner as was done for the axial loading (Figure 44). Finally, torsional loading was applied via a series of step loads of ±3, ±6 and ±9 N-m for 20 sinusoidal cycles at a rate of 0.5 Hz. The loading protocol closely replicated the protocol used by Choi et al (4). Axial, bending and torsional stiffness values were obtained from the slope of the force versus axial displacement, bending moment versus mid-span displacement and torque versus angular displacement curves, respectively. Following testing with the scaffold in place, the scaffold was removed and the same series of tests repeated without the scaffold. The axial

compression, bending and torsion test were randomized. Then a cyclic torsional failure test under torque control was performed, measuring angular rotation in internal and external rotation as a function of increasing torque from 10 N-m to 45 N-m in increments of 5 N-m. Statistical analyses were performed with a 2-way ANOVA test.

The results of the biomechanical tests are provided in Table 3. There is one series of test data for Operation 985L missing because of preliminary torsional failure in the first torsion test. The results show no significant difference for bending or axial stiffness with non-locking vs locking fixation with the scaffold present or absent. Torsional stiffness is significantly higher (p=0.002) with the scaffold present for both non-locking and locking compared to the scaffold absent. In testing to failure, angular rotation is found to be significantly greater in internal rotation (p=0.034) for the non-locking construct than for the locking construct. External rotation was also greater for the non-locking construct, though it did not reach significance (p=0.168). The non-locking construct failed first for 5 of the 6 pairs and at approximately the same number of cycles for the 6th pair. The mode of failure for the non-locking construct varied between catastrophic failure and screw loosening. All locking constructs failed catastrophically, with no screw loosening prior to failure.

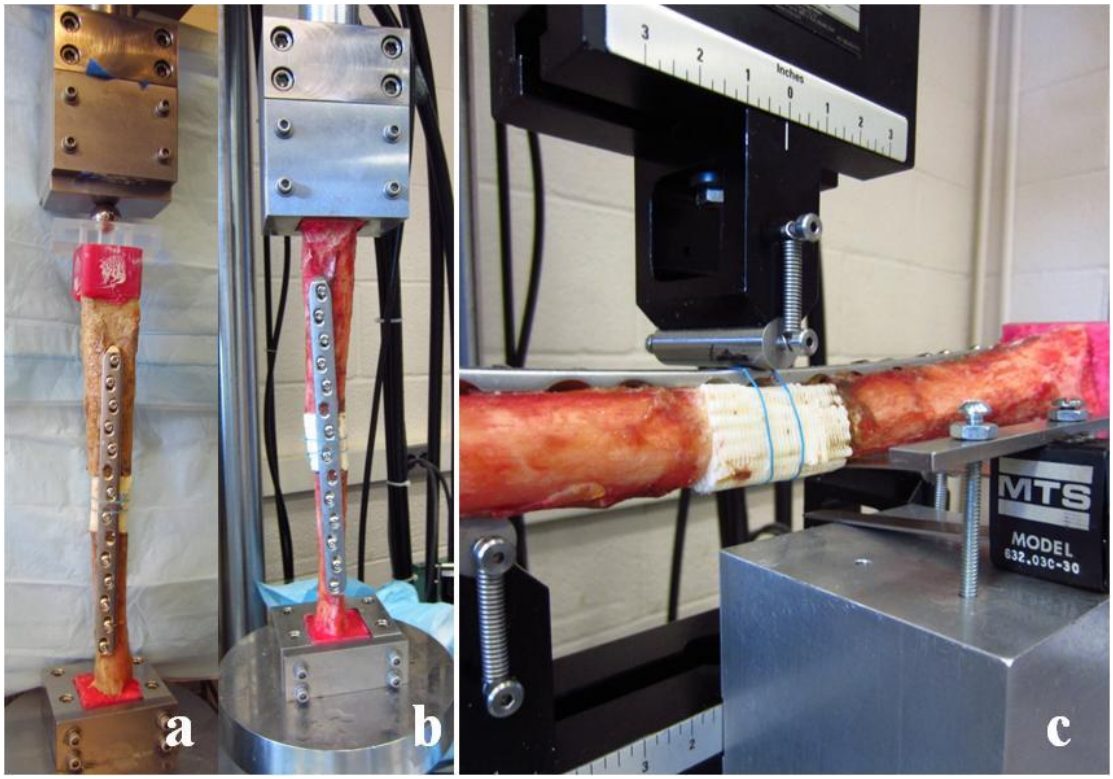

Figure 44: Mechanical testing of human cadaveric tibia with scaffold in segmental defect, (a) axial loading via ball bearing, (b) torsional loading via rectangular block, (c) three-point bending of tibia-plate-scaffold construct, bending load is applied to the middle of the locking plate.

Specimen Number		Screw Type		Axial Compression Stiffness (N*mm)	Torsional Stiffness (N*m*deg)	3-Point Bending Stiffness (N*mm)	Total Energy to Failure (N-m-deg)
979	L	Cortical	scaffold	5358	2.052	212	56396
	L	Cortical	no scaffold	2952	2.005	37	
	R	Locking	scaffold	2525	2.486	938	560
	R	Locking	no scaffold	2369	2.19	551	
980	R	Cortical	scaffold	1518	1.481	1990	30888
	R	Cortical	no scaffold	1337	1.196	1755	
	L	Locking	scaffold	1423	1.785	1495	2706
	L	Locking	no scaffold	1618	1.632	1292	
981	R	Cortical	scaffold	2954	2.194	994	14401
	R	Cortical	no scaffold	2815	2.092	1763	
	L	Locking	scaffold	1868	2.473	676	5503
	L	Locking	no scaffold	1240	2.261	827	
983	L	Cortical	scaffold	1559	2.105	345	5078
	L	Cortical	no scaffold	1597	1.794	166	
	R	Locking	scaffold	1798	1.981	969	14103
	R	Locking	no scaffold	2512	1.798	805	
984	R	Cortical	scaffold	1539	2.637	1367	2362
	R	Cortical	no scaffold	1526	2.404	1020	
	L	Locking	scaffold	1931	2.334	748	4636
	L	Locking	no scaffold	1599	2.175	902	
985	L	Cortical	scaffold				
	L	Cortical	no scaffold				
	R	Locking	scaffold	930	1.533	758	620
	R	Locking	no scaffold	854	1.532	287	

Table 3: Mechanical test results for human cadaveric tibiae with and without scaffolds present in the segmental defects. Axial compression, torsion and three-point bending loading were applied in a randomized sequence. After cyclic loading, the specimens were failed in torsion.

3. KEY RESEARCH ACCOMPLISHMENTS

3.1 All 3 pilot osteochondral defect (Aim 1) dogs went through the full 16 week recovery period. Upon sacrifice and dissection, the osteochondral implants were found to be very well fixed in the surrounding bone, supporting the key design of the osteochondral implant and ingrowth of the surrounding bone.

3.2 Hard sectioning histology demonstrated tissue in growth in both the osteochondral and segmental defect dogs.

3.3 The PCL+HA mixture used to construct the scaffold has been optimized (all three Aims).

3.4 Ten segmental defect surgeries (Aim 2) were performed and 5 out of 7 animals successfully completed the full 16 weeks post-surgery recovery period with the remaining 3 dogs currently doing very well.

3.5 Outcome measures for osteochondral defect dogs (Aim 1) and segmental defect dogs (Aim 2) demonstrated that the surgical procedure was well-tolerated by the dogs and did not impair their quality of life.

3.6 There was no immune response by any of the animals to the poly-caprolactone (PCL) and hydroxyapatite (HA) scaffolds (Aims 1 and 2).

3.7 Surgeries for three out of the five arms of the segmental defect group (Aim 2): unseeded scaffolds (5), canine allografts (2), BMP-2 seeded scaffolds (3); have been performed

3.8 The biomechanical testing protocol and methodology for segmental defect (Aim 2) tibiae is working well.

3.9 Biomechanical testing demonstrated that the PCL-HA scaffold can perform similarly to that of a cadaveric canine allograft.

3.10 The component of human cadaveric testing (Aim 3) in support of Aim 2 was completed. A complementary study comparing locking to non-locking plates was also completed.

4. REPORTABLE OUTCOMES

Two abstracts based on the results of this project were accepted for presentation at the 2014 Annual Meeting of the Orthopaedic Research Society in New Orleans, LA. The first abstract, "Tissue Engineering Massive Osteochondral Defects with Anatomically Matched PCL-HA Scaffolds in a Dog Model" reports our findings related to Aim 1 of this project. The second abstract, "Comparison of PCL-HA Scaffolds to Allografts for Implantation in Critical Size Segmental Tibial Defects in a Canine Model" reports our results related to Aim 2 of this project. Both abstracts are included in the Appendix.

5. CONCLUSIONS

Surgeries have been carried out on a total of thirteen dogs (3 osteochondral defects (Aim 1), 10 segmental defects (Aim 2), nine during this reporting period. Mechanical testing was performed on five of the segmental defect dogs, three are still in the recovery period and testing could not be conducted on two of the dogs because of early sacrifices due to plate failure. A slightly different plate is now being used following mechanical testing that confirmed that the new plate resulted in a much stronger plate/bone construct.

Though no soft tissue was observed to grow on the articular surfaces of the scaffolds in the three osteochondral dogs, this was not a surprising finding since these were unseeded scaffolds. However, all three dogs confirmed that the osteochondral scaffold material was well tolerated in the knee joint, and the scaffold design was incorporated into the surrounding bone, resulting in a very stable implant.

Hard histology was performed for both the osteochondral and segmental defect dogs which showed connective tissue ingrowth into both scaffolds when adjacent to native bone.

The outcome measures and imaging modalities (radiographs and MR) demonstrated consistent results between measurement metrics and with clinical observations. They are felt to form a solid quantitative and qualitative approach to accurately assessing the results of surgical interventions.

Mechanical testing of the human cadaveric analog of the time zero case of the segmental defect (Aim 3) was completed. The presence of the scaffold was found to have no effect for bending or axial loading, and a slight effect in torsion. When comparing a locking construct to a non-locking construct, the non-locking construct was found to have greater compliance to internal rotation than that of the locking construct. The implication of this testing is that the bone/plate construct is sufficiently strong without the need for additional load support from the scaffold and that this construct is mechanically stable at time zero, even without surrounding soft tissue support. Furthermore, the locking screw construct resulted in a less compliant construct than the non-locking screw construct.

5.1 So What

The torsional testing of the segmental defect dogs showed failure strengths for the unseeded scaffolds that were comparable to that of the gold standard allografts. It is expected that with BMP-2 and/or canine MSC seeded scaffolds, the resulting strength of the construct will be even greater. The osteochondral scaffold design demonstrated that it integrates well with the surrounding femoral condyle and will serve as a good platform to test the efficacies of the scaffold to grow cartilage when seeded with TGF-β and/or canine MSCs. Therefore, continued funding of this effort is felt to be justified to complete the full experimental design to demonstrate if *in vivo* large animal translational experiments will lead

to the development of new military technology products and utilities for the definitive and preventive orthopaedic care of military personnel and retirees.

6. REFERENCES

1. Rohrer MD, Schubert CC. The cutting grinding technique for histologic preparation of undecalcified bone and bone-anchored implants. Oral Surg Oral Med Oral Pathol. 1992;74:73-8.
2. Lee CH, Cook JL, Mendelson A, Moioli EK, Yao H, Mao JJ. Regeneration of the articular surface of the rabbit synovial joint by cell homing: a proof of concept study. Lancet. 2010;376(9739):440-8.
3. Moioli EK, Hong L, Mao JJ. Inhibition of osteogenic differentiation of human mesenchymal stem cells. Wound Rep Reg. 2007;15:413-21.
4. Choi JK, Gardner TR, Yoon E, Morrison TA, Macaulay WB, Geller JA. The effect of fixation technique on the stiffness of comminuted Vancouver B1 periprosthetic femur fractures. The Journal of arthroplasty. 2010;25(6 Suppl):124-8.

7. APPENDICES

Control/Tracking Number: 2014-A-1156-ORS
Activity: ORS Annual Meeting Abstract Submission
Current Date/Time: 9/12/2013 11:09:30 AM

Tissue Engineering Massive Osteochondral Defects with Anatomically Matched PCL-HA Scaffolds in a Dog Model

Author Block Hanying Bai, Ph.D[1], Chandhanarat Chandhanayingyong, M.D.[2], Thomas R. Gardner, MCE[2], Chang H. Lee, PhD[2], George C. Vorys, MD[1], Saqib Nizami, BS[2], Jeremy J. Mao, DDS, PhD[3], Francis Y. Lee, M.D. Ph.D.[2].
[1]Columbia University Medical Center, New York, NY, USA, [2]Columbia University, New York, NY, USA, [3]Dental Medicine Growth & Development Center, Columbia University Medical Center, New York, NY, USA.

Abstract:
Introduction: Large osteochondral defects remain an extremely challenging problem to orthopaedic surgeons. Current treatment options include arthroscopic debridement, microfracture, and autograft or allograft OATS. These techniques are not suitable for massive defects though. Recently there has been interest in tissue engineering techniques with the use of scaffolds. Fabricated scaffolds can be designed for optimal shape, size and strength to fit the bony defect. In addition, scaffolds mimicking bone morphology can enhance bone regeneration. Hydroxyapatite (HA, Ca10(PO4)6(OH)2) is known for its similarity to natural bone and is frequently used in the fabrication of porous and inter-connected scaffolds. HA is biocompatible but difficult to incorporate with biological agents. Combining HA with polymers such as PCL (Polycaprolactone) can overcome this problem. This PCL- HA complex has the advantages of enhanced mechanical stability, easy-processing and biodegradability. We present a novel design for reconstruction of a massive femoral defect in a dog model using an anatomically correct scaffold.
Methods: The anatomic contour of the native mongrel medial femoral condyle was acquired from computed tomography (CT) scans of cadaver dog legs. The CT scans were converted to a 3-dimensional model allowing manipulation in CAD (Mimics, Materialise). A scaffold utilizing the medial femoral articular surface with a keeled base plate for implantation was designed. Scaffolds were fabricated from a polycaprolactone hydroxyapatite polymer (PCL-HA) using a 3D bioprinter (Bioplotter, EnvisionTec, Germany). The scaffold has a biphasic design with a superficial cartilage layer with 400 μm interconnecting microchannels to promote articular cartilage growth, and a second deeper layer with 200 μm microchannels to support bony ingrowth

from the surrounding subcondral bone as previously described by the co-authors in a small animal model. Three mongrel dogs (22.5 Kg) were utilized. A standard medial parapatellar approach was performed. A 1.4 ×1.2 ×0.5 cm defect from the medial femoral condyle was cut enbloc with a mini sagittal saw. A trough of 1.0 × 0.8 × 0.5 cm was created in the medial condyle using osteotomes to accommodate to the keel of the scaffold. The scaffold was press-fit in place. Postoperatively, the specimens were evaluated at 4, 8, 12 and 16 weeks with radiographs and MRI. Behavioral evaluations, such as weight-bearing, lameness, pain upon palpation and knee range of motion according to Table 1 were done five times week throughout the 16 recovery period. Animals were sacrificed at 16 weeks, the femurs carefully dissected out and encased in PMMA blocks for histologic analysis. H&E staining was performed.

Results: Postoperatively, overall scores of two dogs fell in the good range (6~7) and the scores of each separate functional section were above the middle range. The overall scores of the third dog stayed in fair rage (4-5). Clinical measures plateaued for all dogs after approximately 30 days. After sacrifice the ROM of the operative left side was compared to the control right side. The left operative knee averaged 114 deg flexion compared to the control knee 120 deg. Implants were found to well-fixed within all animals at dissection. Histology showed bony ingrowth and incorporation of the scaffold as the mechanism for this fixation. MRI did not indicate any cartilage formation as a function of time and none was observed at dissection.

Discussion: An anatomically correct PCL-HA polymer scaffold was successfully implanted into a massive osteochondral defect without any apparent immune response. It remained stable and allowed ambulation throughout the study period. These unseeded scaffolds demonstrated biologic bony incorporation at the time of sacrifice but did not demonstrate any cartilage formation.

Significance: This novel design polymer scaffold offers a potential option for treatment of massive osteochondral defects. Further investigation with seeding of chondrocytes, mesenchymal stem cells, and/or growth factors such as TGF-B3 is warranted to promote cartilage formation.

Acknowledgments: This work is supported by USAMRMC Grant #OR090175

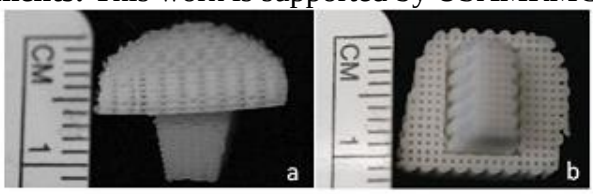

Figure.1 Osteochondral scaffold showing a) side view in superior-inferior direction, b) keel of scaffold

References:

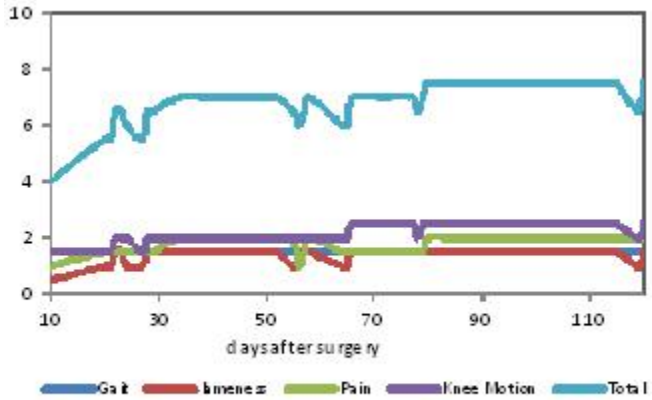

Figure 2 functional outcome measurements for the dogs

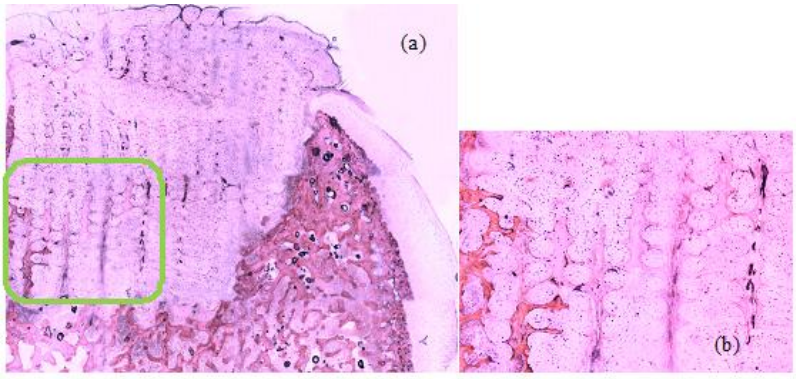

Figure 3 Hard tissue histology (H&E stained) for (a) knee condyle, (b) zoom-in of green region

Outcome	Criteria	Range
Gait	non weight-bearing	0
	partial weight-bearing	1
	full weight-bearing	2
Lameness	does not use limb during walking	0
	partial use of affected limb, walks with noticeable limb	1
	no lameness when walking	2
Pain	severe reaction to touch, withdraws upon the slightest touch with guarding behavior and/or vocalization	0
	mild reaction to touch, withdraws limb upon touch	1
	no reaction to touch of affected limb	2
Knee Motion	significant reduction in range of motion (0-30%)	0
	moderate reduction in range of motion (30-60%)	1
	slightly reduced range of motion (60-80 %)	2
	normal range of motion (90-100%, preoperative range)	3
Total	Excellent: 8-9, Good: 6-7, Fair: 4-5, Poor: <3	0~9

Table 1 functional outcome measurement criteria

Author Disclosure Information: H. Bai: 1; Hanying Bai. **C. Chandhanayingyong:** 1; Hanying Bai. **T.R. Gardner:** 3A; Thomas R. Gardner. **C.H. Lee:** None. **G.C. Vorys:** None. **S. Nizami:** None. **J.J. Mao:** None. **F.Y. Lee:** None.

Control/Tracking Number: 2014-A-2934-ORS
Activity: ORS Annual Meeting Abstract Submission
Current Date/Time: 9/12/2013 11:06:57 AM

Comparison of PCL-HA Scaffolds to Allografts for Implantation in Critical Size Segmental Tibial Defects in a Canine Model

Author Block Hanying Bai, Ph.D[1], Thomas R. Gardner, MCE[1], Chandhanarat Chandhanayingyong, M.D.[2], George C. Vorys, MD[1], Saqib Nizami, BS[2], Chang H. Lee, PhD[2], Jeremy J. Mao, DDS, PhD[3], Francis Y. Lee, M.D. Ph.D.[2].
[1]Columbia University Medical Center, New York, NY, USA, [2]Columbia University, New York, NY, USA, [3]Dental Medicine Growth & Development Center, Columbia University Medical Center, New York, NY, USA.

Abstract:
Introduction: In the treatment of relatively "small" size bony defects, autogenous grafts coming from the iliac crest or tibia are considered the "gold standard". However, this technique has limitations if the bone segmental defect is larger than those-called "critical size" defect. Tissue engineering materials for bone are being developed as an alternative to allografts in part because they lack the potential for an autoimmune response. Fabricated scaffolds can be designed for optimal shape, size and strength to fit the bony defect. In addition, scaffolds mimicking bone morphology can enhance bone regeneration. Hydroxyapatite (HA,

Ca10(PO4)6(OH)2) is known for its similarity to natural bone and is frequently used in the fabrication of porous and inter-connected scaffolds. HA is biocompatible but difficult to incorporate with biological agents. Combining HA with polymers such as PCL (Polycaprolactone) can overcome this problem. This PCL- HA complex has the advantages of enhanced mechanical stability, easy-processing and biodegradability. PCL-HA scaffolds and canine allografts were implanted in the surgically created critical size defects in canine tibia. Clinical outcome measures were recorded for 16 weeks post-surgery and mechanical tests perform following sacrifice to compare the efficacy of the two types of implants to restore ambulation and the resulting mechanical bone strength.

Methods: CT scans of several cadaveric mongrel dog limbs were used to create a 3-D geometric model of dog tibiae and a 2 cm segmental defect was virtually removed from the tibiae. The resulting 3-D computer model of the segmental defect was used to make PCL-HA scaffolds that were fabricated with Bioplotter 3-dimensional printer (EnvisonTec, Germany) with a 25 gauge micro-channel nozzle. Two cm critical size segmental defects were surgically created in the right tibia of seven mongrel dogs (average 22.7 kgf). Five dogs received PCL-HA scaffold implants and two dogs received fresh-frozen canine allograft implants. Two of the scaffold implant dogs experienced surgery related complications and were sacrificed early. A third scaffold implant dog was excluded from mechanical testing due to problems in specimen preparation. The scaffold or allograft implants (Veterinary Transplant Services, Kent, WA) were inserted to snugly fit within the segmental defect and an 8 hole, 105 mm LCP plates (locking compression plates, Synthes Co., USA) was used to fix the transected bone. Six 3.5 mm locking screws were used to fix the plate to the tibia. An oblique 3.5 mm cortical screw was used to further secure the implant and prevent toggling. Following surgery, dogs were sling-walked for several days and then allowed full cage activity for 16 post-surgery period. Radiographs were obtained for all dogs postoperatively at 4, 8, 12 and 16 week healing period. Behavioral evaluations, such as weight-bearing, lameness, pain upon palpation and knee range of motion (Table 1) were recorded 5 days a week for the entire 16 week recovery period. After the full 16 week healing period the dogs were humanely euthanized and both hind limbs were disarticulated at the hip, wrapped in physiologic saline soaked gauze and frozen at -20°C until the day of testing. On the day of testing, the both the experimental (right) and control (left) limbs were thawed to room temperature, the tibiae carefully dissected out and the proximal and distal ends of the tibia potted in polycarbonate blocks secured with 2 diagonal 2.0 mm Kirschner wires (Zimmer, Warsaw IN) and then encased in poly(methyl methacrylate). The tibiae were kept wrapped in physiologic saline soaked gauze throughout the potting process to maintain hydration. Biomechanical testing was performed in an MTS 858 Bionix material testing machine (MTS, Eden Prairie MN) with a biaxial (axial [±5kN]/torsional [± 50 N-m)]) load cell. An internal rotation at a constant rate of 1 N/s was applied to the proximal end of the tibia until failure occurred while the distal end was fixed. Torque, angular displacement, and axial force were collected at 20 Hz. Torque at failure, angular displacement at failure and rotational energy to failure were calculated for both the experimental and control limbs and the ratio of the experimental limb values to the control limb computed for each parameter.

Results: Clinical outcome measures as a function of time for a scaffold dog (Figure 1a) and an allograft dog (Figure 1b) show that both implant types plateaued at approximately the same time and showed very a very similar time course for all outcome measures. Similar results were obtained for the other scaffold and allograft dogs. Ratios of the biomechanical test parameters (experimental/control) in terms of percentage for failure torque, angular rotation at failure and rotational energy to failure are listed in Table 2. Neither the allograft nor scaffold implants fully restored the mechanical strength of the experimental limb to that of the control (non-operated) limb by the end of the 16 week recovery period. However, the mechanical results of the PCL-HA scaffolds for one dog were very comparable to that of the allograft dogs with the other scaffold dog somewhat lower, indicating that it the PCL-HA scaffold can perform similarly to that of an allograft.

Discussion: Preliminary results indicate that the PCL-HA scaffold may be able to serve as a substitute for allografts in the healing of critical size tibial segmental defects both in terms of clinical outcome measures and mechanical strength.

Significance: If additional testing supports these findings, then the PCL-HA scaffold may be able to serve as a low-cost alternative to allografts that allows for optimization of shape and size, with the for potential seeding with biologic agents and/or stem cells without the complications of an immune response.

Acknowledgments: This work is supported by USAMRMC Grant #OR090175

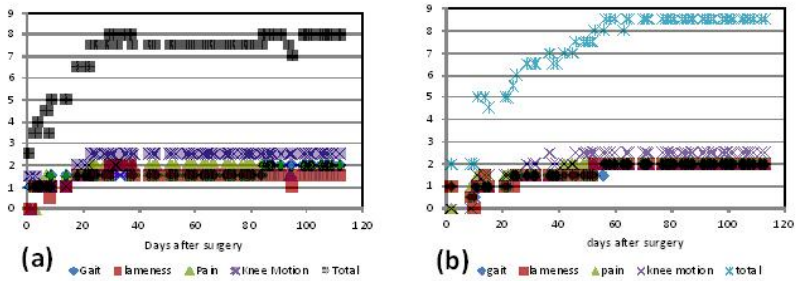

Figure 1, Outcome measurement for (a) scaffold dog 4 and (b) allograft dog 1.

References:

Outcome	Criteria	Range
Gait	non weight-bearing	0
	partial weight-bearing	1
	full weight-bearing	2
Lameness	does not use limb during walking	0
	partial use of affected limb, walks with noticeable limb	1
	no lameness when walking	2
Pain	severe reaction to touch, withdraws upon the slightest touch with guarding behavior and/or vocalization	0
	mild reaction to touch, withdraws limb upon touch	1
	no reaction to touch of affected limb	2
Knee Motion	significant reduction in range of motion (0-30%)	0
	moderate reduction in range of motion (30-60%)	1
	slightly reduced range of motion (60-80 %)	2
	normal range of motion (90-100%, preoperative range)	3
Total	Excellent: 8-9, Good: 6-7, Fair: 4-5, Poor: <3	0~9

Table 1 functional outcome measurement criteria

Animal	Failure Torque	Failure Angular Rotation	Rotational Energy to Failure
Scaffold Dog 2	38.8%	63.1%	24.2%
Scaffold Dog 4	80.1%	78.7%	65.7%
Allograft Dog 1	67.1%	88.6%	61.9%
Allograft Dog 2	82.3%	71.8%	55.7%

Table 2. Ratio of surgical tibia (right) to control tibia (left) as a percentage for measured values.

Author Disclosure Information: H. Bai: None. **T.R. Gardner:** None. **C. Chandhanayingyong:** None. **G.C. Vorys:** None. **S. Nizami:** None. **C.H. Lee:** None. **J.J. Mao:** None. **F.Y. Lee:** None.